ESA Climate Change Initiative (CCI)

Sea Level Budget Closure (SLBC_cci)

Product Description Document D2.1.2
ESA_SLBC_cci_D2.1.2
Version v1.1, issued 27 Sept 2017

Description of data set and uncertainty assessment, version 0

Prime & Science Lead:	Martin Horwath Technische Universität Dresden Martin.Horwath@tu-dresden.de
Technical Officer:	Jerôme Benveniste ESA ESRIN, Frascati, Italy Jerome.Benveniste@esa.int
Consortium:	Laboratoire d'Etudes en Géophysique et Océanographie Spatiales (LEGOS) Universität Bremen (UB) Universität Zürich (UZH) University of Leeds (UoL) Goethe-Universität Frankfurt (GUF) Danmarks Tekniske Universitet, DTU Space, Geodynamics (DTU-GDK) Danmarks Tekniske Universitet, DTU Space, Geodesy (DTU-GEK) Nansen Environmental and Remote Sensing Center (NERSC) University of Reading (UoR)

To be cited as:

Novotny, K.; Horwath, M.; Cazenave, A.; Palanisamy, H.; Marzeion, B.; Paul, F.; Le Bris, R.; Döll, P.; Caceres, D.; Hogg, A.; Shepherd, A.; Forsberg, R.; Sørensen, L.; Andersen, O.B.; Johannessen, J.; Nilsen, J.E.; Gutknecht, B.D.; Merchant, Ch.J.; Macintosh, C.R.: *ESA Climate Change Initiative (CCI) Sea Level Budget Closure (SLBC_cci). Product Description Document D2.1.2: Version 0 data sets and uncertainty assessments. Version 1.2, 27 Sept 2017.*

Signatures page

Prepared by	Kristin Novotny Project Manager, TUDr Martin Horwath Science Leader, TUDr Anny Cazenave, Hindumathi Palanisamy, LEGOS; Ben Marzeion, UB; Frank Paul, Raymond Le Bris, UZH; Petra Döll, Denise Caceres, GUF; Anna Hogg, Andrew Shepherd, UOL; Rene Forsberg, Louise Sandberg Sørensen, DTU-GDK; Ole B. Andersen, DTU-GEK; Johnny Johannessen, Jan Even O. Nilsen, NERSC; Benjamin D. Gutknecht, TUDr; Christopher John Merchant, Claire Rachel Macintosh, UoR	Date: 2017-09-27 K. N
Checked by	Martin Horwath Science Leader, TUDr	Date: 2017-09-27 Martin Horwath
Approved by	Jerôme Benveniste Technical Officer, ESA	Date:

Table of Contents

Change Log

Issue	Author, Org.	Affected Section	Reason/Description	Status
1.0	M. Horwath / TUDr ...	All	Document Creation	Released to ESA 2017-06-28
1.1	K. Novotny, M. Horwath / TUDr	All	Document revision after review by ESA	Released to ESA 2017-09-05

Distribution List

Organization	Consortium Member
TUDr	Martin Horwath
LEGOS	Anny Cazenave
UB	Ben Marzeion
UZH	Frank Paul
UoL	Andrew Shepherd, Anna Hogg
DTU - GDK	Rene Forsberg
GUF	Petra Döll
NERSC	Johnny Johannessen
DTU - GEK	Ole B. Andersen
UoR	Christopher Merchant
ESA	Jérôme Benveniste, Marco Restano, Américo Ambózio

Acronyms and Abbreviations

Acronym	Explanation
AC	Atlas of the Cryosphere
AET	Actual EvapoTranspiration
AIS	Antarctic Ice Sheet
AISCCI	Antarctic Ice Sheet CCI
AOD	atmospheric and oceanic de-aliasing
ASCII	American Standard Code for Information Interchange
ATBD	Algorithm Theoretical Baseline Document
AVISO	Validation and Interpretation of Satellite Oceanographic data
BISICLES	Berkeley Ice Sheet Initiative for Climate Extremes
CCI	Climate Change Initiative (initiated by ESA)
CECR	Comprehensive Error Characterisation Report
CF	Climate and Forecast
COBE	Centennial in situ Observation Based Estimates (sea surface temperature)
GPCC	Global Precipitation Climatology Centre
CRI	Coastline Resolution Improvement
CRU	Climatic Research Unit (University of East Anglia, Norwich, UK)
CRU TS	CRU Timeseries (grids of observed climate)
CRUGPCC	combined climatology data from CRU (temperature, cloudiness, number of days with rain) and GPCC (precipitation)
CSIRO	Commonwealth Scientific and Industrial Research Organization
CSR	Center for Space Research (University of Texas at Austin)
csv	Comma-separated values
CU	Colorado University
DDM	global Drainage Direction Map
DOI	Digital object identifier
DTU	Danmarks Tekniske Universitet
EAIS	East Antarctic Ice Sheet
ECMWF	European Centre for Medium-Range Weather Forecasts
ECV	Essential Climate Variables
ELA	Equilibrium Line Altitude
EN4	version 4 of the Met Office Hadley Centre ‘’EN’’ series of data sets of global quality controlled ocean temperature and salinity profiles
ENVISAT	"Environmental Satellite", Earth-observing satellite operated by ESA
EPSG	European Petroleum Survey Group
EPSG3031	EPSG Projection 3031 - WGS 84 / Antarctic Polar Stereographic
ERA	Earth system ReAnalysis
ERS-1/2	European Remote Sensing Satellite -1/2
ESA	European Space Agency
EWH	equivalent water height

GAA, GAB, GAC, GAD	Names of data products related to GRACE atmospheric and oceanic background models (refer to section 3.2.2)
GDAC	Argo global data assembly centre
GFZ	GeoForschungsZentrum Potsdam
GIA	Glacial Isostatic Adjustment
GIS	Greenland Ice Sheet
GMB	Gravimetric Mass Balance
GMSL	Global Mean Sea Level
GMT	Generic Mapping Tools
GPCC	Global Precipitation Climatology Centre
GPS / GNSS	Global Positioning System / Global Navigation Satellite System
GRACE	Gravity Recovery and Climate Experiment
GrIS	Greenland Ice Sheet
GSFC	Goddard Space Flight Center
GSHHG	Global Self-consistent, Hierarchical, High-resolution Geography Database
GSSL	Global mean Steric Sea Level
GTSPP	Global Temperature and Salinity Profil Program
GWSWUSE	submodel of the WaterGAP WGHM
HDF5	Hierarchical Data Format (HDF)
HIRHAM	RCM based on a subset of the HIRLAM and ECHAM models
HYCOM	Hybrid Coordinate Ocean Model
HYOGA	Japanese, means glacier
ICE-5G, ICE-6G	models of postglacial relative sea-level history
ICESat	Ice, Cloud, and land Elevation Satellite, part of NASA's Earth Observing System
IFREMER	Institut Français de Recherche et d'Exploitation de la MER
IK	steric sea level data set by Ishii and Kimoto (2009) (refer to chapter 2)
IMBIE	Ice Sheet Mass Balance Inter-comparison Exercise
IPRC	International Pacific Research Center
IRD	Institut de Recherche pour le Development (France)
ITSG	Institute of Geodesy, Theoretical Geodesy and Satellite Geodesy (TU Graz)
JAMSTEC	Japan Agency for Marine-Earth Science and Technology
JPL	Jet Propulsion Laboratory
KVS	Updated version of the global mean steric time series computed by von Schuckmann and Le Traon (2011) (refer to chapter 2)
LEGOS	Laboratoire d'Etudes en Géophysique et Océanographie Spatiales
MBT	Mechanical Bathythermograph
MD5	"Message Digest" (MD), MD5 algorithm can be used as a checksum to verify data integrity
MOG2D	Modèle d'Onde de Gravité à 2 Dimensions
MSS	mean sea surface
NA	net abstractions
NERSC	Nansen Environmental and Remote Sensing Center

NOAA	National Oceanographic and Atmospheric Administration
NSIDC	National Snow and Ice Data Center
OBP	Ocean Bottom Pressure
OMC	Ocean Mass Change
OMCT	Ocean Model for Circulation and Tides
PGR	post-glacial rebound
PSD	Product Specification Document
PUG	Product User Guide
RA	Radar Altimetry
RCM	Regional atmospheric Climate Model
RGI	Randolph Glacier Inventory
RWR	Renewable Water Resources
SARAL	Satellite with ARgos and ALtiKa, cooperative altimetry technology mission of Indian Space Research Organisation (ISRO) and CNES (Space Agency of France)
SCRIPPS	Scripps Institution of Oceanography (University of California)
SEC	Surface Elevation Change
SELEN	SEa Level EquatioN solver
SH	spherical harmonic
SLA	sea level anomaly
SL_cci	ESA CCI_Sea Level Project
SLBC	Sea Level Budget Closure
SSL	Steric Sea Level
SSL4SLBC	Steric Sea Level for Sea Level Budget Closure
T/S	Temperature/Salinity
TOPAZ	(Towards) an Operational Prediction system for the North Atlantic European coastal Zones
TOPEX	TOPography EXperiment, part of the TOPEX/Poseidon satellite(joint radar altimetry project, NASA and CNES)
TS	Time Series
TUDr	Technische Universität Dresden
TWS	Total Water Storage
UL	University of Leeds
UP	The ICE6g (Peltier et al., 2015 - refer to sec. 5.5) rate of radial displacement (UPlift)
VM	model of the radial viscoelastic structure of the Earth (used fo ICE-5G)
w.e.	water equivalent
WAIS	West Antarctic Ice Sheet
WATCH	The WATer and global CHange project
WDBII	CIA World Data Bank
WFD	WATCH Forcing Data
WFDEI	Watch Forcing Data based on ERA-Interim reanalysis
WGHM	WaterGAP Global Hydrology Model

WGMS	World Glacier Monitoring Service
WGS84	World Geodetic System 1984
WOA	World Ocean Atlas
WOD	World Ocean Database
WP	Work Package
WVS	World Vector Shorelines
XBT	Expendable Bathythermograph

1. Introduction

1.1. Purpose and Scope

This document describes the Version 0 (v0) datasets on individual sea level budget components. V0 products have been gathered in the initial phase of the SLBC_cci project to reflect the situation at the beginning of the project, prior to any improvement and further adaptation. This implies that some inconsistencies exist and that the degree of detail in the description varies depending on whether the consortium partners are authors of the described products or have acquired them from other sources. The document (Deliverable D2.1.2), together with the set of related datasets (D2.1.1) hence forms the starting point and reference for further analyses and improvements.

1.2. Document Structure

Section 2 to 7 contain the descriptions for the sea level and steric component, the ocean mass component, the glacier contribution, the ice sheet contribution, the land water contribution, and the dedicated datasets for the Arctic area, respectively. Each section has the same subdivision into subsections describing sources of the datasets, algorithms, product specification, uncertainty assessments, and finally the reference list.

University of Reading (UoR) contributes to this project within SSL4SBC_cci. Data provided by UoR are described in detail in the respective Product Description Document 1 (ESA_SSL4SLBC_cci_D2.1.2). For the sake of completeness this document is attached at the end.

1.3. Data Structure

All data described in this documentation are stored at a project's data drive at TU Dresden. Access is managed by Kristin Novotny (Kristin.Novotny@tu-dresden.de).

Data files are organized in the following structure:

```
/Data_v0
    /WP211_gmsl_steric_v0
    |       /Data_LEGOS
    |       |       GMSL_AVISO.nc
    |       |       GMSL_CCI.nc
    |       |       GMSL_CSIRO.nc
    |       |       GMSL_CU.nc
    |       |       GMSL_GSFC.nc
    |       |       GMSL_NOAA.nc
```

GSSL_EN4.nc
GSSL_IK6_13.nc
GSSL_IPRC.nc
GSSL_JAMSTEC.nc
GSSL_KVS.nc
GSSL_NOAA.nc
GSSL_SCRIPPS.nc
grid_sla_aviso.nc
grid_sla_CCI_V2_0.nc
grid_steric_EN4.nc
grid_steric_IK6_13.nc
grid_steric_IPRC.nc
grid_steric_JAMSTEC.nc
grid_steric_NOAA.nc
grid_steric_SCRIPPS.nc

/Data_UnivReading

KvS_Steric_height_timeseries_v0.nc
KvS_Steric_height_v0.nc
nceo_l3s_sst.nc
nceo_timeseries.n

/WP221_ocean_mass_v0

/CSR_Mascons

CSR_GRACE_RL05_Mascons_v01.nc

/GSFC_Mascons

GSFC_mascons_HDF5_format.pdf
GSFC_ocean_mascons_v02.2_OBP-GeruoA.h5

/JPL_Mascons_CRI

/mass_variability_time_series

antarctica_mass_200204_201608.txt
greenland_mass_200204_201608.txt
ocean_mass_200204_201608.txt

CLM4.SCALE_FACTOR.JPL.MSCNv01CRIv01.nc
CLM4.SCALE_FACTOR.JPL.MSCNv01CRIv01.nc.md5
GRCTellus.JPL.200204_201608.GLO.RL05M_1.MSCNv02CRIv02.nc
GRCTellus.JPL.200204_201608.GLO.RL05M_1.MSCNv02CRIv02.nc.md5
JPL_MSCNv01_PLACEMENT.nc
LAND_MASK.CRIv01.nc
LAND_MASK.CRIv01.nc.md5
README_byJpl.txt

/OcMassChangeGridsSLBCv0

EWH_OcMassChangeGrid_CSR_SLBC_1x1.nc
EWH_OcMassChangeGrid_CSR_SLBC_5x5.nc
EWH_OcMassChangeGrid_GSFC_SLBC_1x1.nc
EWH_OcMassChangeGrid_GSFC_SLBC_5x5.nc
EWH_OcMassChangeGrid_ITSG_SLBC_1x1.nc
EWH_OcMassChangeGrid_ITSG_SLBC_5x5.nc

EWH_OcMassChangeGrid_JPL_SLBC_1x1.nc
EWH_OcMassChangeGrid_JPL_SLBC_5x5.nc
README.txt

/OcMassTimeSeriesSLBCv0

ArcticOceanMassTimeSeries_CSR_mascon.csv
ArcticOceanMassTimeSeries_GSFC_mascon.csv
ArcticOceanMassTimeSeries_ITSG60_300kmbuffer_scaled.csv
ArcticOceanMassTimeSeries_JPL_mascon.csv
CHAMBERS__ocean_mass_orig.txt
OceanMassTimeSeries_CSR_mascon.csv
OceanMassTimeSeries_GSFC_mascon.csv
OceanMassTimeSeries_ITSG60_300kmbuffer_scaled.csv
OceanMassTimeSeries_JPL_mascon.csv
README.txt

README_overview.txt

/WP231_glaciers_v0

glaciers_cru_324_rgi_v5.nc

/WP241_icesheets_v0

/AIS_Altim

SLBC_RA_EAIS_mass_1992_2016.csv
SLBC_RA_WAIS_mass_1992_2016.csv

/AIS_GMB

AIS_GMB_basin.dat
AIS_GMB_grid.dat
AIS_GMB_grid.nc
AIS_GMB_grid.tif
AIS_GMB_trend.dat

/GIS_Altim

SLBC_ICEsat_mass_2003_2009.txt

/GIS_GMB

GIS00_grace.dat
GIS01_grace.dat
GIS02_grace.dat
GIS03_grace.dat
GIS04_grace.dat
GIS05_grace.dat
GIS06_grace.dat
GIS07_grace.dat
GIS08_grace.dat
README.txt

/WP251_tws_v0

/global_tws

WaterGAP22b_CRU_version0_month1992_2014.txt
WaterGAP22b_CRU_version0_year1992_2014.txt
WaterGAP22b_CRU_version0_yearinmonth1992_2014.txt
WaterGAP22b_CRUGPCC_version0_month1992_2014.txt
WaterGAP22b_CRUGPCC_version0_year1992_2014.txt

WaterGAP22b_CRUGPCC_version0_yearinmonth1992_2014.txt
WaterGAP22b_WFDbcWFDEI_version0_month1992_2014.txt
WaterGAP22b_WFDbcWFDEI_version0_year1992_2014.txt
WaterGAP22b_WFDbcWFDEI_version0_yearinmonth1992_2014.txt
global_average_tws_without_greenland.xls

/gridded_tws

tws_WaterGAP22b_WFDEIhom_version0.nc
tws_WaterGAP22b_WFDEIhom_version0.nc4

/WP261_ArcticOcean

/Data_DTUGEK_Altim

Arc_SLA_*YYYYMM*.dat.gz with *YYYY-MM*=1992-09 … 2014-08

/Data_NERSC

topazssh20032015.nc
topazstht20032015.nc

2. Total Sea Level and Steric Sea Level Change

Data described in the following section are provided by LEGOS, Toulouse. In addition, University of Reading (UoR) contributes to this project within SSL4SBC_cci. Data provided by UoR are described in detail in the respective Product Description Document 1 (ESA_SSL4SLBC_cci_D2.1.2) which is also attached to this document.

2.1. Data access and requirements

Altimetry-based sea level data

Different sources of products are available. Six different products from five processing groups are considered for the altimetry-based sea level data:

(1) Validation and Interpretation of Satellite Oceanographic data (AVISO)
(2) Colorado University (CU)
(3) National Oceanographic and Atmospheric Administration (NOAA)
(4) Goddard Space Flight Center (GSFC)
(5) Commonwealth Scientific and Industrial Research Organization (CSIRO)
(6) The Climate Change Initiative (CCI) sea level data

The above mentioned altimetry sea level data can be accessed from the following websites.

(1) AVISO:
http://www.aviso.altimetry.fr/en/data/products/ocean-indicators-products/actualitesindicateurs-des-oceansniveau-moyen-des-mersindexhtml.html
(2) Colorado University (CU Release):
http://sealevel.colorado.edu/
(3) National Oceanographic and Atmospheric Administration (NOAA):
http://www.star.nesdis.noaa.gov/sod/lsa/SeaLevelRise/LSA_SLR_timeseries_global.php).
(4) Goddard Space Flight Center (GSFC version 2):
http://podaac-ftp.jpl.nasa.gov/dataset/MERGED_TP_J1_OSTM_OST_GMSL_ASCII_V2)
(5) Commonwealth Scientific and Industrial Research Organization (CSIRO):
www.cmar.csiro.au/sealevel/sl_data_cmar.html)
(6) The Climate Change Initiative (CCI) sea level data:
ftp://slcci@ftp.esa-sealevel-cci.org/SeaLevel-ECV/V2.0_20161205.

General information on the data are given at the webpage http://www.esa-sealevel-cci.org/, access to the data directory (password) can be got by e-mail as stated on the web page.

Steric data

Various sources of steric data are considered:

XBT-based steric sea level time series

For the period January 1993-December 2004 the following three data sets have been computed at LEGOS based on Expandable Bathy Thermograph (XBT) data:

(1) the updated versions of Ishii and Kimoto (2009)
(2) NOAA data set (Levitus et al., 2012)
(3) EN4 data set (Good et al., 2013).

Argo data set

As of January 2005, four Argo temperature and salinity data sets are available for the project from the following institutes/team:

(1) International Pacific Research Center (IPRC)
(2) Japan Agency for Marine-Earth Science and Technology (JAMSTEC)
(3) SCRIPPS Institution of Oceanography (SCRIPPS)
(4) Updated version of the global mean steric time series computed by von Schuckmann and Le Traon (2011) (0-1500m ocean layer).

The above steric sea level data can be accessed from the following websites.

XBT data

(1) Ishii and Kimoto (2009) data set (called IK hereinafter): we used the updated v6.13 version available at http://rda.ucar.edu/datasets/ds285.3/.
It is based on the World Ocean Database 2005 and World Ocean Atlas 2005 (WOD05 and WOA05), the Global Temperature-Salinity in the tropical Pacific from the Institut de Recherche pour le Development (IRD, France), and the Centennial in situ Observation Based Estimates (COBE) sea surface temperature. The XBT depth bias correction is applied in the current version. The temperature and salinity data are available at monthly interval over 24 depth levels ranging from the ocean surface down to 1500 m depth, on a global 1° x 1° grid from January 1945 to December 2012 (see Ishii and Kimoto, 2009, for details).

(2) NOAA data set: available at https://www.nodc.noaa.gov/OC5/3M_HEAT_CONTENT.
As described in Levitus et al. (2012), this 1°x1° data set uses the World Ocean Database 2009 (WOD09) plus additional data processed since 2009. Bias corrections are applied to the Mechanical Bathy Thermograph (MBT) and XBT data as described by Levitus et al. (2009). The temperature and salinity grids below 700 m and with a maximum depth of 2000 m are not available prior to January 2005.

(3) EN4 data set: we used the EN4.0.2 version from Met Office Hadley Centre (http://www.metoffice.gov.uk/hadobs/en4/download-en4-0-2.html).
This data set is based on quality controlled subsurface ocean temperature and salinity profiles and objective analyses. The EN4.0.2 data set is an incremental development of the previous EN2 and EN3 versions. Data sources include the WOD09, Global Temperature and Salinity Profil Program (GTSPP) and Argo data from Argo global data assembly centres (GDACs). The EN4.0.2 temperature and salinity data are corrected for the XBT and MBT bias. The temperature and salinity data are available at monthly interval over 40 depth levels ranging from the ocean surface down to 5350 m depth, on a global 1° x 1° grid from January 1900 to December 2013. Details on the data processing are given in Good et al. (2013).

Except for the NOAA data set for which steric sea level grids are directly available, for the other data sets, we have computed the steric sea level time series integrating the T/S data over the 0-2000 m depth range. The global mean steric time series were further estimated by geographically averaging the gridded data.

For the whole set of time series, annual and semi-annual cycles were removed and residual time series were smoothened using a 3-month moving window.

Argo data

The following are the data access sources for Argo data sets

(1) The International Pacific Research Center (IPRC; http://apdrc.soest.hawaii.edu/projects/Argo/data/gridded/On_standard_levels/index-1.html)
(2) The Japan Agency for Marine-Earth Science and Technology (JAMSTEC; ftp://ftp2.jamstec.go.jp/pub/argo/MOAA_GPV/Glb_PRS/OI/).
(3) The SCRIPPS Institution of Oceanography (SCRIPPS; http://sio-argo.ucsd.edu/RG_Climatology.html)
(4) von Schuckmann and Le Traon (2011) (0-1500m ocean layer).

These data sets are available at monthly interval on a global 1° x 1° grid down to 2000 m, over the period January 2005 to December 2015.

The steric sea level time series (and associated uncertainty; but note that only Jamstec provides errors) are computed over January 2005-December 2015, integrating the T/S data over the 0-2000 m depth range. The global mean steric time series from IPRC, Jamstec and SCRIPPS are estimated over the 62.5°S–64.5°N, 60.5°S–66°N and 61.5°S–64.5°N domains, respectively. We also used an updated version of the steric data set processed by von Schuckmann and Le Traon (2011). This data set provides steric sea level and associated uncertainty based on quality controlled Argo temperature and salinity data from IFREMER (http://wwz.ifremer.fr/lpo_eng/content/view/full/83074), with integration down to 2000 m depth and averaging on a 5°x10° grid. Their method is described in detail in von Schuckmann and Le Traon (2011). In the following, we call this data set 'KVS'. The KVS data set covers the 60°S-60°N domain. Area weighting is applied to all data sets when averaging.

It is clear from figure 2 that discrepancies among data sets are much larger for the XBT data. This comes from the poorer coverage of this data set and differences adopted by the processing groups to fill the gaps in the data and interpolation methodologies. It remains that the XBT data sets do not contain any information on ocean temperature below 700 m. This has to be borne in mind when comparing thermal expansion before and after 2005.

2.2. Algorithms

2.2.1. Review of scientific background

Altimetry-based sea level

The AVISO, CU, NOAA, GSFC and CSIRO sea level data sets are based on TOPEX/Poseidon, Jason-1 and Jason-2 data averaged over the 66°S - 66°N domain, except for the CSIRO data averaged over 65°S to 65°N. For each product, a set of instrumental and geophysical corrections is applied (details are given on the websites of each data set). In addition, the effect of Glacial Isostatic Adjustment (GIA, i.e. a small correction of -0.3mm/yr, Peltier 2004) is accounted for in each sea level time series except in the NOAA data set. Thus the latter sea level data was corrected for the GIA effect, using the -0.3 mm/yr value. The sea level time series used in this study cover the period January 1993 - December 2015.The five sea level time series (AVISO, CU, GSFC, NOAA and CSIRO) are obtained either by directly averaging the along-track sea surface height data (e.g., CU) or by firstly gridding the unevenly distributed along track data and then performing grid averaging (e.g., AVISO and NOAA). In all cases, an area weighting is applied. In addition to the geographical averaging method, other differences exist between the sea level data sets because of the applied geophysical & instrumental corrections and the number of satellites considered (e.g., Masters et al., 2012, Henry et al., 2014).

Figure 1 shows global mean sea level time series from satellite altimetry. The temporal period of the altimetry data is between January 1993 and December 2016. While the global mean sea level time series are provided by all the 5 processing groups, the gridded sea level products are from AVISO and CCI. The gridded data sets provided here are at monthly interval on a global 1°x1° grid between 90°N-90°S.

In the context of the European Space Agency/ESA Climate Change Initiative/CCI 'Sea Level' project, a new improved product has been computed. It combines data from the TOPEX/Poseidon, Jason-1/2 and CryoSat-2 with the ERS-1/2 and Envisat missions and is

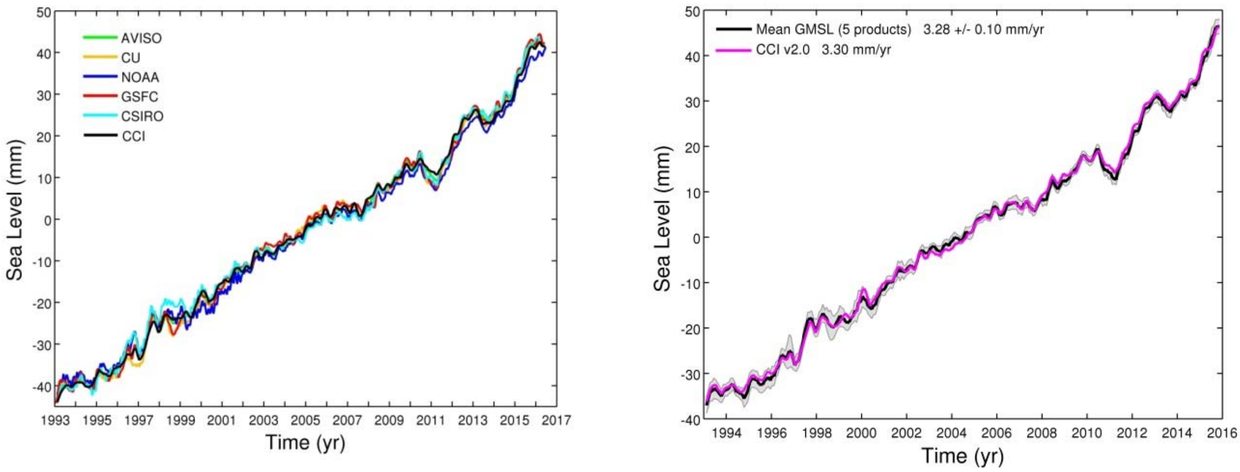

Figure 1: Global mean sea level time series from satellite altimetry over January 1993-December 2015. Left: products from the 6 processing groups. Right: average of AVISO, CU, NOAA, GSFC and CSIRO, with the CCI product superimposed.

based on a new processing system with dedicated algorithms and adapted data processing strategies (Ablain et al., 2015, 2017). The main improvements include: reduction of orbit errors and wet/dry atmospheric correction errors, reduction of instrumental drifts and bias, inter-calibration biases, inter-calibration between satellite altimetry missions and combination of the different sea level data sets, and an improvement of the reference mean sea surface. The CCI sea level products have been validated using different approaches; including a comparison with tide gauge records as well as to ocean re-analyses and climate model outputs (see Ablain et al., 2015, 2017 for more details). The CCI sea level data (version v2.0) set is freely available over January 1993 - December 2015.

The first version of the Sea Level Climate Change Initiative (SL_cci) products was initially distributed in September 2012. A full reprocessing of the sea level ECV has been produced and is now available for the users. This v2.0 dataset covers the period Jan. 1993 to Dec. 2015.

The CCI 'Sea Level' data set is a multi-satellite merged product that consists in a database of different elements that can be referenced with the following DOI: 10.5270/esa-sea_level_cci-1993_2015-v_2.0-201612.

Within the SL_cci project, the estimation of the sea level has been improved in the Arctic Ocean. A sea level Arctic product (maps of sea level anomalies) based on the Envisat and SARAL/AltiKa missions has been produced and is available for the users.

The description of some specific technical issues related to the corrections and algorithms used in the SL_cci products can be found in the list of publications on the CCI_sea level website.

Steric data

Refer to Section 2.2 for respective scientific backgrounds.

2.2.2. Algorithms

Refer to Section 2.2.1. In addition, the algorithm involved in the computation of the altimetry based sea level estimates (ESA-CCI sea level in specific) can be found in the ATBD of SL_CCI website http://www.esa-sealevel-cci.org/PublicDocuments/Technical. The file name is SLCCI-ATBDv1-016-3-3.pdf .

2.3. Product Specification

2.3.1. Product geophysical data content

Altimetry sea level data

Files listed below contain values of sea level anomaly. Sea level anomaly, also called sea surface height anomaly is the sea surface height with reference to a mean sea surface or mean profile.

(1) Global mean sea level data

The products have the naming format: **GMSL_XX.nc**

XX → AVISO; CU; NOAA; GSFC; CSIRO; CCI

Geophysical Variable	**Name in product**	**Unit**
Global mean sea level anomaly	gmsl	mm
Time	time	Decimal year

(2) Gridded sea level data

The products have the naming format: **grid_sla_XX.nc**

XX → CCI_V2_0; aviso

Geophysical Variable	**Name in product**	**Unit**
Sea level anomaly	sla	mm
Time	time	Decimal year
Longitude	lon	degree
Latitude	lat	degree

Steric data

(1) Global mean steric sea level data

The products have the naming format: **GSSL_XX.nc**

XX → KVS; IPRC; EN4

Geophysical Variable	Name in product	Unit
Global mean steric sea level anomaly	gssl	mm
Time	time	Decimal year
GSSL error	error	mm

XX → IPRC; SCRIPPS; NOAA; IK6_13

Geophysical Variable	Name in product	Unit
Global mean steric sea level anomaly	gssl	mm
Time	time	Decimal year

(2) Gridded steric sea level data

The products have the naming format: **grid_steric_XX.nc**

XX → JAMSTEC; NOAA; EN4

Geophysical Variable	Name in product	Unit
Steric sea level anomaly	steric	mm
Time	time	Decimal year
Longitude	lon	degree
Latitude	lat	degree
Error	error	mm

XX → IPRC; SCRIPPS

Geophysical Variable	Name in product	Unit
Steric sea level anomaly	steric	mm
Time	time	Decimal year
Longitude	lon	degree
Latitude	lat	degree

XX → IK6_13

Geophysical Variable	Name in product	Unit
Steric sea level anomaly	steric	mm
Time	time	Decimal year
Error	error	mm

(3) Steric ocean heights from University of Reading

files provided: KvS_Steric_height_timeseries_vo.nc
KvS_Steric_height_vo.nc
nceo_l3s_sst.nc
nceo_timeseries.nc

For file information and file content please refer to *Steric Sea Level for Sea Level Budget Closure (SSL4SLBC_cci), Product Description Document 1* given in the appendix.

2.3.2. Coverage and resolution in time and space

Sea level data

The AVISO and CCI sea level grids are given at monthly interval with a spatial resolution of ¼ degree over the 66S-66N and 82S-82N domains over January 1993 to December 2015 respectively. A global mean sea level time series at monthly interval over January 1993 to December 2015 are also available.

All the XBT and 3 Argo based (IPRC, JAMSTEC, SCRIPPS) steric sea level grids are available at 1 degree resolution over time periods explained in Section 2.2. Schuckmann and Le Traon (2011) provide averaged Argo data on a 5x10 degree grid.

2.3.3. Product data format

Data are available in netCDF4 format.

2.3.4. Product grid and projection

/

2.4. Uncertainty Assessment

2.4.1. Sources of error

Altimetry-based GMSL

Although currently errors of the GMSL time series are not provided by the processing groups, the source of errors have been abundantly discussed in many articles (Ablain et al., 2015, 2017, Dieng et al, 2015a, b, 2017). We do not reproduce these discussions here. We just summarize the current sources of errors in the tables below (Table 1 and Table 2).

For the steric data, some time series are provided with errors (for XBT data, only the Ishii and Kimoto data set and EN4 give errors; for Argo, errors are provided for the Jamstec, and KVS) (Figure 2).

Table 1: Sources of errors for GMSL trend estimation (Ablain et al., 2015)

Source	Trend errors (mm/yr)
Orbit error	~0.25
Wet troposphere correction (instrumental drift of onboard radiometers)	~0.3
Intrumental altimeter bias (Topex A-Topex B)	~0.25
Dry troposphere correction (uncertainty of atm. surface pressure data)	~0.1
Sea state bias correction	~0.1
Total error	*~0.4*
Tide gauge calibration (e.g. Mitchum et al., 2010)	~0.4

Table 2: Uncertainties of CCI sea level products (Ablain et al., 2015):

Sea Level Uncertainty of CCI products

Spatial Scales	Temporal Scales	GCOS Requirements	Errors of CCI products
Global Mean Sea Level	Long-term trend	<0.3 mm/yr	~ 0.3 mm/yr
	Interannual signals	0.5 mm over 1 year	< 2 mm over 1 year
Regional Sea Level	Long-term trend	<1 mm/yr	<2 mm/yr (except for western boundary currents)
	Interannual signals	Not Defined	Not evaluated

Source: Ablain et al., 2015

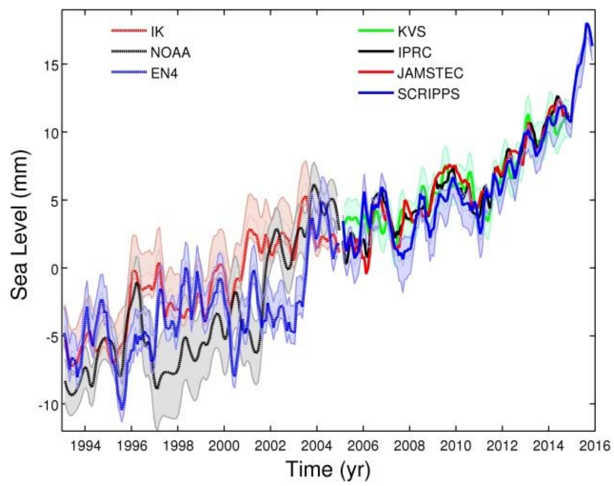

Figure 2: Global mean steric sea level time series from from IK, NOAA and EN4 (integration down to 700 m) over January 1993–December 2004 and Argo-based (integration down to 2000 m) from four processing groups (KVS, IPRC, JAMSTEC and SCRIPPS) over January 2005–December 2014 (extended until December 2015 with the SCRIPPS data). Shaded areas represent the data uncertainties.

2.4.2. Methodology for uncertainty assessment

See section 2.4.4.

2.4.3. Results of uncertainty assessment

See section 2.4.1 and 2.4.4.

2.4.4. Uncertainty documentation in the data products

See source articles.

2.5. References

Ablain, M., Cazenave, A., Larnicol, G., Balmaseda, M., Cipollini, P., Faugère, Y., Fernandes, M. J., Henry, O., Johannessen, J. A., Knudsen, P., Andersen, O., Legeais, J., Meyssignac, B., Picot, N., Roca, M., Rudenko, S., Scharffenberg, M. G., Stammer, D., Timms, G., and Benveniste, J. (2015), Improved sea level record over the satellite altimetry era (1993–2010) from the Climate Change Initiative project, *Ocean Sci*., 11, 67–82, doi:10.5194/os-11-67-2015.

Ablain M., Legeais J. F., Prandi P., Marcos M., Fenoglio-Marc L., Dieng H. B., Benveniste J. and Cazenave A. (2017), Altimetry-based sea level at global and regional scales. *Surv. Geophys*., 38, 7-31, doi: 10.1007/s10712-016-9389-8.

Dieng H., Palanisamy H., Cazenave A., Meyssignac B. and von Schuckmann K. (2015a), The sea level budget since 2003: inference on the deep ocean heat content, *Surveys in Geophysics*, 36, 1, doi:10.1007/s10712-015-9314-6.

Dieng H., Cazenave A., von Shuckmann K., Ablain M. and Meyssignac B. (2015b): Sea level budget over 2005-2013: missing contributions and data errors, *Ocean Science*, 11, 1-14, doi:10.5194/osd-11-1-2015b.

Dieng H., Cazenave A., Meyssignac B. and Ablain M., New estimate of the current rate of sea level rise from a sea level budget approach, *Geophys. Res. Lett*., 44, doi:10.1002/2017GL073308, 2017.

Good, S. A., Martin, M. J., and Rayner, N. A. (2013): EN4: quality controlled ocean temperature and salinity profiles and monthly objective analyses with uncertainty estimates, *J. Geophys. Res.Oceans*, 118, 6704–6716, doi:10.1002/2013JC009067.

Henry O., Ablain M., Meyssignac B., Cazenave A., Masters D., Nerem S., Leuliette E. and Garric G. (2014): Investigating and reducing differences between the satellite altimetry-based global mean sea level time series provided by different processing groups, *J. Geodesy*, 88, 351–361, doi:10.1007/s00190-013-0687-3.

Ishii, M., and M. Kimoto (2009), Reevaluation of historical ocean heat content variations with time-varying XBT and MBT depth bias corrections, *J. Oceanogr.*, *65*(3), 287–299, doi:10.1007/s10872-009-0027-7.

Levitus S., J.I. Antonov, T.P. Boyer, O.K. Baranova, H.E. Garcia, R.A. Locarnini, A.V. Mishonov, J.R. Reagan, D. Seidov, E.S. Yarosh and M.M. Zweng (2012), World ocean heat content and thermosteric sea level change (0-2000 m), 1955-2010, *Geophys. Res. Lett*., 39, L10603, doi:10.1019/2012GL051106.

Levitus S, Antonov JI, Boyer TP, Locarnini RA, Garcia HE, Mishonov AV (2009): Global ocean heat content 1955-2008 in light of recently revealed instrumentation problems. *Geophysical Research Letters* 36:L07608.

Masters, D., Nerem, R. S., Choe, C., Leuliette, E., Beckley, B., White, N., and Ablain, M. (2012): Comparison of global mean sea level time series from TOPEX/Poseidon, Jason-1, and Jason-2, Mar. Geod., 35, 20–41.

Peltier, W. R. (2004) : Global glacial isostasy and the surface of the ice-age Earth: the ICE-5G (VM2) model and GRACE. *Annu. Rev. Earth Planet. Sci.*, 32, 111-149.

von Schuckmann, K. and Le Traon, P.-Y. (2011): How well can we derive Global Ocean Indicators from Argo data?, Ocean Sci., 7, 783–791, doi:10.5194/os-7-783-2011.

3. Ocean Mass Change

Time-variable ocean mass products are derived from monthly solutions from the Gravity Recovery And Climate Experiment (GRACE) satellite mission (Tapley et al. 2004). While the processing and inversion approaches of the products involved differ considerably, the common setting is such that mass redistributions in the Earth-/Ocean system cause changes in the gravity field that become observed with the GRACE satellites. Here, these changes are expressed as temporal changes of mass per surface area in kg/m^2 near the Earth's surface, or equivalently, temporal changes of *equivalent water height (EWH)* in millimeters water equivalent (mm w.e.). The changes are expressed relative to an arbitrary reference state, e.g. the temporal mean state over the GRACE period. The EWH is a *hypothetical* layer of fresh water which would cause the observed change in gravity at each data point, respectively.

3.1. Data Access and Requirements

The following products are considered:

CSR Mascons

Institution: Center for Space Research, University of Texas at Austin
Product source: http://www2.csr.utexas.edu/grace/RL05_mascons.html
Reference: Save et al. 2016

JPL Mascons

Institution: Jet Propulsion Laboratory (NASA)
Product Source: http://grace.jpl.nasa.gov/data/get-data/jpl_global_mascons/
Reference: Watkins et al. 2015

GSFC Mascons

Institution: Goddard Space Flight Center (NASA)
Product Source: http://ssed.gsfc.nasa.gov/grace
Reference: Luthcke et al. 2013

Don Chambers' global mean ocean mass change time series

Product Source:
https://dl.dropboxusercontent.com/u/31563267/ocean_mass_orig.txt
Reference: Johnson and Chambers (2013); Chambers and Bonin (2012)

ITSG-Grace2016-based grids

Institution: Institut für Geodäsie, TU Graz

Product Source: https://www.tugraz.at/institute/ifg/downloads/gravity-field-models/itsg-grace2016/

Reference: Klinger et al. 2016, Mayer-Gürr et al. 2016

Note: The grids are generated by TU Dresden based on the ITSG-Grace2016 spherical harmonic solution series, involving additional processing and filtering steps. The solution series ITSG-Grace2016 was chosen for this purpose because previous evaluations of the quality of available solution series have indicated that ITSG-Grace2016 exhibits the lowest noise level while apparently retaining all geophysical signal (Horwath & Groh 2016).

3.2. Algorithms

3.2.1. Review of scientific background

Global solutions of Earth's gravity field are commonly represented by the coefficients (so-called Stokes coefficients) of a spherical harmonic (SH) expansion up to a specific maximum SH degree (Wahr et al. 1998). GRACE processing centers typically analyze Level-1 GRACE data (including the GRACE K-band ranging data, on-board GPS data and accelerometer data) to estimate a set of Stokes coefficients on a monthly basis („monthly SH solutions").

Following the "atmospheric and oceanic de-aliasing" (AOD) approach, modelled short-term atmospheric and oceanic mass variations (as well as tidal mass variations) are accounted for as part of the background model within the gravity field estimation procedure (Flechtner et al. 2014, Dobslaw et al. 2013). Therefore, these variations are not included in the monthly solutions. In order to retain the full mass variation effect in the ocean domain, the respective monthly averages of the AOD fields need to be added back to the monthly solutions. These monthly averages are provided by the analysis centers of the GRACE Science and Data System. They have adopted the following nomenclature for those products: GAA products for the atmospheric mass variations, GAB products for the oceanic mass variations, and GAC products for the sum of the two. As an additional series of products, GAD products contain the sum of atmospheric surface pressure effects and ocean mass effects over the ocean domain (advised for comparisons with ocean bottom pressure observations). Different options of restoring mass variations in the oceanic domain exist for different oceanic applications of GRACE (compare section "De-aliasing products and ocean-only mascons" in the GSFC mascon description at https://ssed.gsfc.nasa.gov/grace/products.html).

GRACE is insensitive to surface mass displacement components of SH degree one (mass exchange between hemispheres). Swenson et al. (2008) have proposed an approach to derive the degree-one components by combining the GRACE information for degree n>=2 with ocean model output. This approach is widely applied. GRACE has also a reduced sensitivity to the C20 component of the gravity field (dynamic flattening term). Therefore, GRACE-based C20 components are commonly replaced by results from satellite laser ranging. Specifically, the mascon solutions by CSR, JPL and GSFC as well as the spherical harmonic-based results by D. Chambers all follow the approach of adding degree-one terms and replacing C_20 in the way described here – see related references given in Section 3.1.

The task of determining changes in the mass distribution from changes of Earth's exterior gravity field has no unique solution. Uniqueness can be enforced by the assumption that the mass redistribution occurs in terms of surface mass changes in a "thin" layer on the Earth surface, comprising the hydrosphere, atmosphere and cryosphere. In this way, global grids of surface mass variations can be calculated from the temporal variations of the gravity field.

Mass redistribution processes in the Earth interior, in particular glacial isostatic adjustment (GIA) or seismic events, cannot be subsumed in the concept of surface load changes. Therefore, they need to be corrected prior to the conversion of gravity field changes to surface mass changes. This is usually done by using results from geophysical modelling.

Due to the attenuation of short wavelength (= high SH degree) gravity field patterns with height, the sensitivity of GRACE rapidly decreases with SH degree. In other words, GRACE errors increase with SH degree. On top of this general error characteristics, GRACE errors exhibit distinct correlation patterns, which show up as north-south striping features and are related to the orbital geometry. In consequence, GRACE analyses for temporal surface mass change involve filtering (spatial smoothing) leading to spatial resolutions limited to 300-500 km. Advanced filter approaches (Swenson and Wahr, 2006; Kusche, 2007) account for the complex, non-isotropic GRACE error structure.

Based on grids of surface mass changes (generated by involving filtering as well as the corrections mentioned above), the total mass change over an area (e.g. the global ocean) is derived by spatial integration with an appropriate weight function. (Equivalently, a respective linear functional may be applied in the spherical harmonic domain.) The reduced spatial resolution causes leakage effects: Mass changes in coastal regions cannot be uniquely assigned to either the land side or the ocean side of the coastline. Since hydrological (or glaciological) changes on the land side tend to have larger amplitudes than oceanic mass changes on the ocean side, a buffer zone of a few hundred kilometers is typically masked out from the ocean integration kernel.

Mascon approaches are a way to enforce a sharp separation between mass changes on either side of coastlines. Mascons (mass concentrations) are direct parameterizations of (localized) surface mass anomalies. Level-1-based mascon solutions directly estimate mascon magnitudes from the Level-1 GRACE data, without involving global gravity field solutions as an intermediate step. Geographically dependent constraints on the spatio-temporal variance and covariance of mass changes can be employed to assign the mass changes to either side of coastlines.

Similar mascon approaches can be followed based on SH gravity field solutions as intermediate ("pseudo-observation") products. This becomes even more attractive when realistic error variance-covariance information of the SH solutions is accounted for. In this way SH solution-based mascon approaches are a flexible way of accounting for incorporating both signal covariance information and error covariance information, without the burden of complete Level-1 data processing.

3.2.2. Algorithms

CSR Mascons RL05

The CSR mascon solution (Save et al. 2016) is a 1° equal area mascon solution based on Level-1 GRACE data. The mascons are defined on a geodesic grid. Tikhonov regularization is applied. No information from geophysical models is introduced for this regularization, but the ocean and the continents are treated as distinct domains. Subsequently, results are interpolated to a 0.5° x 0.5° regular geographic grid. This latter grid is distributed.

Degree one components are added from the data set based on Swenson et al. (2008) and are freely available at ftp://podaac.jpl.nasa.gov/allData/tellus/L2/degree_1/deg1_coef.txt. Only a functional fit (linear and seasonal components) of those coefficients is used.

C_{20} is replaced by results from satellite laser ranging (Cheng et al. 2013).

GAD is restored (according to netcdf meta data).

GIA is removed using GIA modeling results from (A et al. 2013) who in turn use the ICE-5G glaciation history from Peltier (2004).

For the SLBC_cci v0 data package, time series of total ocean mass change are derived from the mascon grids by TUDr. The weighted integral over all oceanic points is calculated using a land-ocean mask extracted with the Generic Mapping Tools (GMT) from the GSHHG (formerly GSHHS) coastline database, which is compiled from the three sources World Vector Shorelines (WVS), CIA World Data Bank (WDBII), and Atlas of the Cryosphere (AC).

JPL Mascons JPL-RL05M

The JPL mascon solution (Watkins et al. 2015) is a global spherical cap mascon solution based on GRACE Level-1 data. Stochastic a priori information is introduced based on near-global geophysical models.

A Coastline Resolution Improvement (CRI) filter is applied to separate the land and ocean portions of mass within each land/ocean mascon in a post-processing step.

Degree one components are added from the data set based on Swenson et al. (2008) and are freely available at ftp://podaac.jpl.nasa.gov/allData/tellus/L2/degree_1/deg1_coef.txt

C_{20} is replaced by results from satellite laser ranging (Cheng et al. 2013).

GAD is restored. Note that this is not explicitly mentioned in the documentation, meta data etc., but the product is labeled: "applicable for ocean, hydrology, and ice applications".

GIA is removed using GIA modeling results from A et al. (2013) who in turn use the ICE-5G glaciation history from Peltier (2004).

For the SLBC_cci v0 data package, time series of total ocean mass change are derived from the mascon grids by TUDr. The weighted integral over all oceanic points is calculated using a land-ocean mask based on the GMT coastline.

GSFC Mascons v2.2

The GSFC v2.2 mascon solution (Luthcke et al. 2013) is a global equal area (1 arc-degree) mascon solution based on Level-1 GRACE data. Anisotropic constraints on the signal covariance were applied.

Degree one components are added from the data set based on Swenson et al. (2008) and are freely available at ftp://podaac.jpl.nasa.gov/allData/tellus/L2/degree_1/deg1_coef.txt

C_{20} is replaced by results from satellite laser ranging (Cheng et al. 2013).

Different versions, w.r.t. GIA corrections and re-addition of signal components are published. For the SLBC_cci v0 purposes, the "GSFC_ocean_mascon_v02.2_OBP-GeruoA" variant is chosen.

The treatment of atmospheric and oceanic background models is such that it is as similar as possible to the respective treatment used for the CSR Mascons and JPL Mascons.

This treatment is complicated by the fact that GSFC uses a different set of background models (namely, ECMWF for the atmosphere and MOG2D for the ocean) than the members of the GRACE Science and Data System CSR and JPL (which use ECMWF for the atmosphere but OMCT for the Ocean). To reach consistency, the difference between the background models was first accounted for by adding ECMWF+MOG2D and subtracting GAC, and subsequently, GAD was restored.

GSFC provides an additional variant (GSFC.ocn.200301_201607_v02.3a_SLA-GeruoA) where the global ocean average of GAD is subtracted in addition, in order to account for changes of the integrated atmospheric masses over the ocean domain. This step will need to be considered in the course of the SLBC_cci project consistently between the different products.

GIA is removed using GIA modeling results from (A et al., 2013) who in turn use the ICE-5G glaciation history from Peltier (2004).

Time series of total ocean mass change are derived by the weighted integral over all oceanic points using an ocean-land mask provided by GSFC specific to the GSFC Mascon solutions.

Chambers' global ocean mass change time series.

The time series result from applying the "direct approach" (cf. Section 3.2.1) to series of global SH GRACE solutions.

Degree one components are added from the data set based on Swenson et al. (2008) and are freely available at ftp://podaac.jpl.nasa.gov/allData/tellus/L2/degree_1/deg1_coef.txt .

C_{20} is replaced by results from satellite laser ranging (Cheng et al. 2013).

GAD is restored.

A 300 km buffer along the coastlines of continents and large islands is applied. The distributed data sets report mean ocean mass change in kg/m² (or mm water equivalent). For the Figures derived in this report, these values were multiplied with the total ocean surface area to convert them into total ocean mass change.

ITSG-Grace2016-based grids

ITSG-Grace2016 (Klinger et al. 2016; Mayer-Gürr et al. 2016) is a series of monthly global SH gravity field solutions. Methodological advancements of the processing by TU Graz include the co-estimation of daily variations (in order to reduce leakage from short-term variations into the monthly solutions) and the incorporation of temporal instrument error covariances. Here we use the series of solutions expanded up to SH degree 60.

These SH solutions are further processed at TU Dresden to derive global grids of surface mass changes.

GAD is restored.

GIA is removed using GIA modeling results from (A et al., 2013) who in turn use the ICE-5G glaciation history from Peltier (2004).

Degree one components are added from the data set based on Swenson et al. (2008) and are freely available at ftp://podaac.jpl.nasa.gov/allData/tellus/L2/degree_1/deg1_coef.txt.

C_{20} is replaced by results from satellite laser ranging (Cheng et al. 2013).

Filtering with the Swenson filter (Swenson and Wahr, 2006) and an additional 300km Gaussian filter is applied.

Gravity field variations are converted into variations of surface mass (cf. 3.2.1). Time series of total ocean mass change are derived by the weighted integral over all oceanic points. For this integration, a 300 km buffer is applied along the ocean margins to avoid leakage from land mass change. The integral is subsequently scaled by the ratio between total ocean area and the integrated area (i.e. total ocean area minus buffer area).

3.3. Product specification

3.3.1. Product geophysical data content

Mascon solutions from CSR, GSFC, and JPL are taken as provided by the institutions. Data are in NetCDF format (except GSFC). Detailed explanations and data content can be found at the related websites (see also section 3.1).

CSR Mascons

File: CSR_GRACE_RL05_Mascons_v01.nc
Product source: http://www2.csr.utexas.edu/grace/RL05_mascons.html

GSFC Mascons

Files: GSFC_mascons_HDF5_format.pdf (HDF5 format summary)
GSFC_ocean_mascons_v02.2_OBP-GeruoA.h5
Product Source: http://ssed.gsfc.nasa.gov/grace

JPL Mascons

Files: GRCTellus.JPL.200204_201701.GLO.RL05M_1.MSCNv02CRIv02.nc
GRCTellus.JPL.200204_201701.GLO.RL05M_1.MSCNv02CRIv02.nc.md5
Product Source: http://grace.jpl.nasa.gov/data/get-data/jpl_global_mascons/

Auxiliary Files (please refer to product website):
CLM4.SCALE_FACTOR.JPL.MSCNv01CRIv01.nc / ~nc.md5
JPL_MSCNv01_PLACEMENT.nc
LAND_MASK.CRIv01.nc nc / ~nc.md5

Time series of mass variability (Ascii/Text-files)
Files: XXX_mass_200204_201608.txt
with XXX ... antarctica, greenland
Content: column description (content, unit)
col 1: TIME (year.decimal)
col 2: XXX mass (Gigatonnes)
col 3: XXX mass 1-sigma uncertainty (Gigatonnes)
File: ocean_mass_200204_201608.txt
Content: column description (content, unit)
col 1: TIME (year.decimal)
col 2: Ocean mass (mm of sea level height)
col 3: Ocean mass 1-sigma uncertainty (mm of sea level height)
col 4: Ocean mass deseasoned (mm of sea level height)

Ocean Mass Change Grids SLBCv0

Files: EWH_OcMassChangeGrid_XXX_SLBC_nxn.nc
with XXX ... CSR, GSFC, ITSG, JPL
and nxn ... resolution 1° by 1° (1x1), 5° by 5° (5x5)

Product source (for ITSG data):
https://www.tugraz.at/institute/ifg/downloads/gravity-field-models/itsg-grace2016/

Content (all files)

Geophysical Variable	Name in product	Unit
change in ocean mass	EWH	kg/m^2 (corresponds to mm w.e.)
Time	time_dec	Decimal year
Longitude	lon	degree_east
Latitude	lat	degrees_north
Error	error	mm

In addition to the gridded products, times series of ocean mass data are provided as text files (comma-separated values, csv).

Files: ArcticOceanMassTimeSeries_XXX_mascon.csv
with XXX ... CSR, GSFC, ITSG, JPL
ArcticOceanMassTimeSeries_ITSG60_300kmbuffer_scaled.csv

OceanMassTimeSeries_XXX_mascon.csv
with XXX ... CSR, GSFC, ITSG, JPL
OceanMassTimeSeries_ITSG60_300kmbuffer_scaled.csv

Content: column description (content, unit)
col 1: TIME (year.decimal)
col 2: mass (ocean mass minus mean_OceanMass) (Gigatonnes)

File: CHAMBERS__ocean_mass_orig.txt
Product Source:
https://dl.dropboxusercontent.com/u/31563267/ocean_mass_orig.txt

Content: column description (content, unit)

col 1: TIME (year.decimal)

col 2-4: Mean ocean mass (in mm of equivalent mean sea level)

col 2: CSR, col 3: GFZ, col 4: JPL

col 5: standard error

Please note comments stated in header of the file!

3.3.2. Coverage and resolution in time and space

CSR Mascons:

- EWH given in cm
- Time is given in days since 2002-01-01
- Period: 2002-04 - 2016-06
- Grid: 0.5° x 0.5° (from 1°x1° - at the equator - equal area geodesics grid)

JPL mascons

- EWH given in cm
- Time is given in days since 2002-01-01
- Period: 2002-04 - 2016-06
- Grid: 0.5° x 0.5° (from 3° - at the equator - equal area spherical caps). The data are represented on a ½ degree lon-lat grid, but they represent the 3x3 degree equal-area caps, which is the current native resolution of JPL-RL05M.

GSFC mascons v2.2

- EWH given in cm
- Time is given in days since 2002-01-00 => 2001-12-31
- Period: 2003-01 - 2016-03
- 41168 1.01° x 1.01° equal area mascons

Homogenization of spatial grid resolution for SLBC_cci

In addition to the generic format of the individual solution series, the CSR-, JPL-, GSFC- and ITSG solution series were interpolated onto the grid formats defined for SLBC_cci:

- EWH given in mm (equivalent to kg/m^2, assuming a water density of 1000 kg/m^3)
- 1° x 1° geographic grid over the ocean
- 5° x 5° geographic grid over the ocean
- Time is given in decimal years
- Periods are identical to the original data sets.

3.3.3. Product data format

Time series of integrated mass changes (global and Arctic north of 66°N) are given as ASCII formatted CSV- and TXT files.

Time series of gridded mass changes are given in the netCDF-4 classic format.

3.3.4. Product grid and projection

The product grids are described in section 3.3.2 (coverage and resolution).

3.4. Uncertainty assessment

3.4.1. Sources of error

GRACE errors: Errors in the GRACE observations as well as in the modeling assumptions applied during GRACE processing propagate into GRACE results on surface mass redistribution and in particular into GRACE-based ocean mass change products ("GRACE errors"). GRACE errors need to be damped in some way, either by filtering (in the case of approaches starting from a SH solution) or by applying regularization methods (in the case of mascon approaches). The loss of spatial resolution implied by approaches to reduce GRACE errors causes leakage errors, in turn (see below).

Errors in C_{20} and degree-one terms are a particular contribution to "GRACE errors", since the C_{20} and degree-one components are usually derived by employing observations and modeling approaches other than GRACE (see Section 3.2.1). Because of their very large scale nature and possible systematic effects (including possible systematic errors in linear trends), errors of these components are particularly important for global ocean mass change applications. The related uncertainties are likely in the order of 0.1 – 0.2 mm/yr (cf. Quinn and Ponte 2010 for degree-one term uncertainty effects).

Leakage errors arise from the vanishing sensitivity of GRACE to small spatial scales (high SH degrees) or, respectively, by the necessity to dampen GRACE errors at small spatial scales. Leakage errors can be described as errors in correctly assigning gravity field changes to the geographic location of surface mass changes. For the case of ocean mass applications, the crucial assignment is to either the land side or the ocean side of coastlines. The problem is aggravated by the fact that surface mass changes on the land side (continental hydrology or continental ice mass changes) are often significantly larger than ocean mass changes. Differences in methods to avoid (or repair) leakage effects can amount to a several tenths of mm w.e./yr in regional OMC estimates (e.g. Kusche et al. 2016).

Uncertainty of corrections: GIA. GRACE alone cannot distinguish between mass redistributions in the ocean and mass redistributions in the underlying solid Earth due to GIA. Therefore, GIA effects are usually corrected based on geophysical GIA models. Current models show strong discrepancies. Therefore, the impact of GIA is among the fundamental uncertainties of GRACE-based ocean mass changes. The uncertainty is on the order of 0.3 mm/yr, and it is correlated to GIA-based uncertainties of altimetry-based GMSL changes and to GIA-based uncertainties in GRACE based ice sheet mass changes (Quinn & Ponte 2010, Chambers et al. 2010, Tamisiea 2011, Rietbroek et al. 2016).

Uncertainty of corrections: Others. Other corrections, with their specific uncertainties, include the correction for rotational feedback effects (Polar tides) to long-term mass redistributions, and corrections for atmospheric mass variations.

3.4.2. Methodology of uncertainty assessment

In addition to the review given in Section 3.4.1, here we show results from a preliminary analysis of the different v0 products. The revealed differences highlight current uncertainties in GRACE-based ocean mass changes.

3.4.3. Results of uncertainty assessment

Figure 3 shows a global map of the linear trend based on the CSR mascons, the JPL mascons, the GSFC mascons and the ITSG-Grace2016 SH solutions expanded up to degree 60. Figure 4 shows the absolute harmonic annual signal amplitude based on the same four solutions.

Figure 5 shows time series of globally integrated ocean mass change from the four series, and, in addition, Chambers' global ocean mass time series. Linear trend estimates (in terms of mean sea level) range from 1.08 to 2.18 mm w.e./yr. Some differences (e.g. the low value from the CSR mascons) can be explained by the preliminary nature of this quick analysis (see below).

Analyses specific to the Arctic Ocean (Region north of 66°N) are shown in Figure 6 (linear trends) and Figure 7 (time series of integrated mass change).

Finally, Figure 8 shows the pairwise differences of geographically distributed linear mass trends of the four solutions.

The figures with geographical maps indicate the common signals in all time series, but also show distinct differences in spatial resolution, in noise structures and in leakage effects and the attempts to mitigate leakage effects.

For example, the JPL mascons, although delivered in a formal 0.5° x 0.5° resolution, show 3° x 3° blocks of equal values, which reflect the 3° resolution of the underlying mascons. At coastlines, however, a 0.5° resolution is attained by the subsequent application of a "coastline resolution enhancement filter".

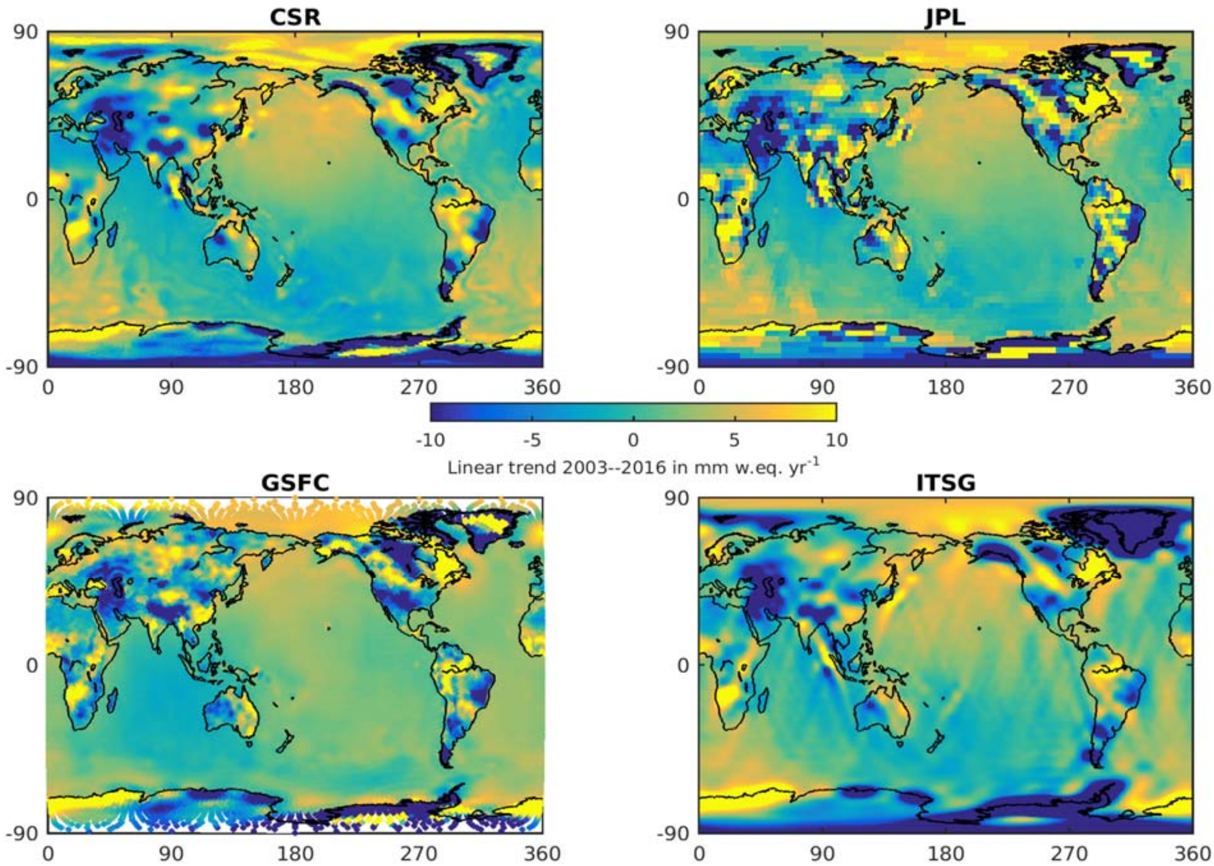

Figure 3: Global linear trends of equivalent water height between 2003 and 2016. The trend was estimated by a least-squares fit of a constant, a linear trend, and annual and semi-annual cosine and sine signals. The SH-based ITSG solution was used in its version up to degree 60.

The CSR and GSFC mascons exhibit a smooth spatial variability between their mascons. The variability tends to be somewhat larger for the CSR mascons than for the JPL and GSFC mascons – see, e.g. the alongated patterns in the Arctic Ocean (Fig. 6) or the structures in the Southern Atlantic (Fig 3). It remains open – at this stage – to what extent these features of the CSR mascon solutions reflect true variability in ocean mass change distribution or artifacts.

The definition of coastlines, or in other words, land-ocean masks, is another important aspect that is treated differently by the different mascon solutions and that needs to be accounted for in more detail in the course of the project. JPL and GSFC deliver respective mask files. However, for the GSFC (see, e.g. Figure 6, Canadian Arctic Archipelago region), mascons seem to be assigned to the land domain when their area just touches a little piece of land. A similar statement is true for the CSR mascons. For the preliminary spherically harmonic-based results shown here, the Gaussian filtering implies that mass changes on land leak into the ocean, which is alleviated by the applied 300 km buffer (cf. Figure 6). The sharper separation between land and ocean mass change based on the spherical harmonic solutions will be realized in the course of the project.

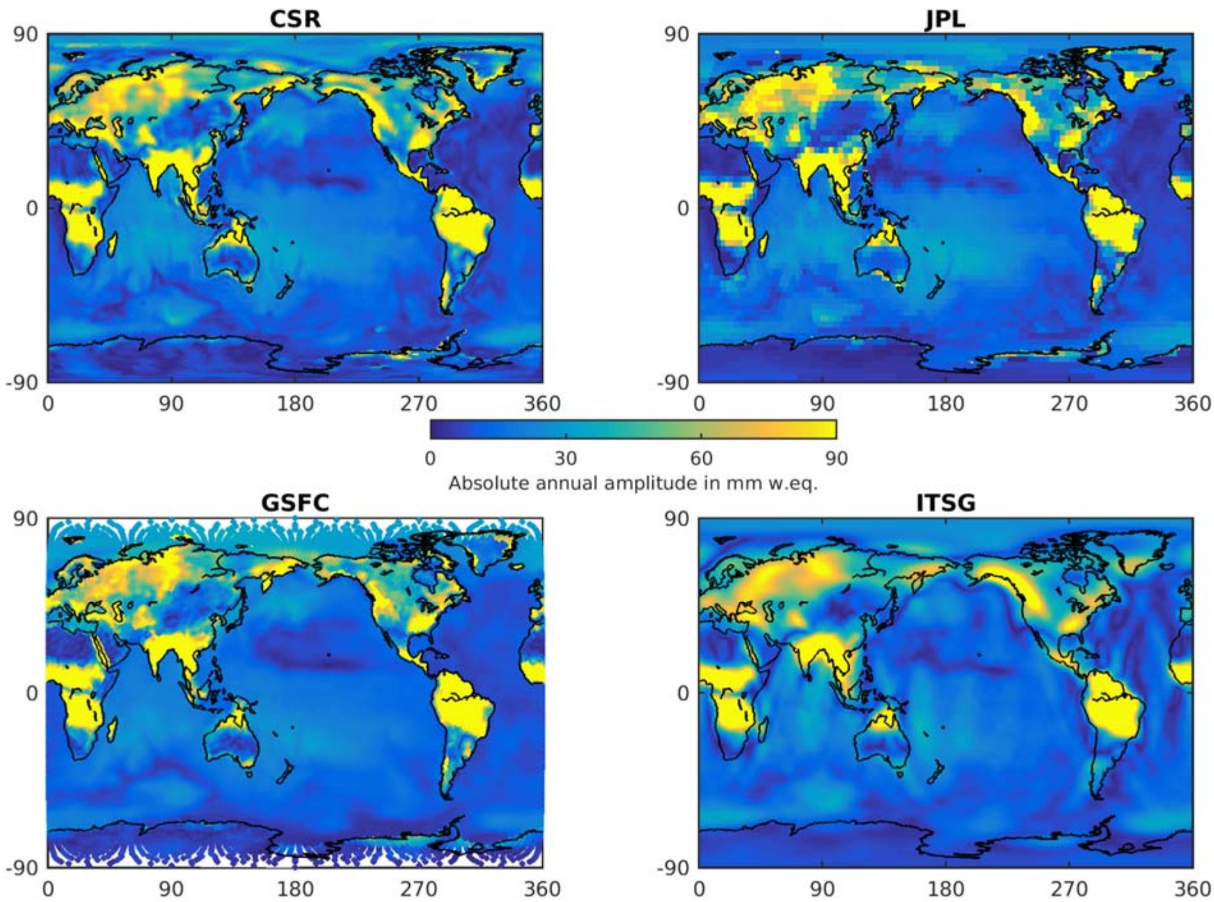

Figure 4: Absolute annual amplitude in an adjustment of up to semi-annual terms, i.e. sqrt(AnnualCosine^2 + AnnualSine^2).

While the different characteristics will need to be accounted for in the further analysis, it cannot be stated that any of the solutions performs generally "better" or "worse" than the others.

Anyway, some implications of the different characteristics for the preliminary results on integrated ocean mass change may be discussed:

Due to the fact that the land-ocean mask used by the CSR mascons tends to extend land areas into the ocean, our analysis (by not yet accounting for this fact) likely counts some mass changes as oceanic mass changes that are actually assigned to land area by the CSR mascon analysis. The resulting leakage from Greenland and Canadian Arctic glacier mass loss is a likely cause for our CSR-based integrated ocean mass change (Figure 7) to be less positive than the respective result from the other series. In fact, the linear trends shown in Figure 7 show a considerable spread in Arctic Ocean mass trends ranging from -1.58 to +4.30 mm w.e./yr, in terms of the contribution to Arctic mean sea level change.

Figure 8 shows that differences between linear trends not only appear in the small-scale noise and small-scale spatial signal attribution, as discussed so far. In addition, a global pattern (SH degree 2 and order 1) shows up in the differences between the GSFC mascon solutions and all other solutions. E.g. in the Pacific, this pattern has opposite sign North and South of the equator, respectively. This pattern is likely related to the different treatment of the pole tide effect (Wahr et al. 2015).

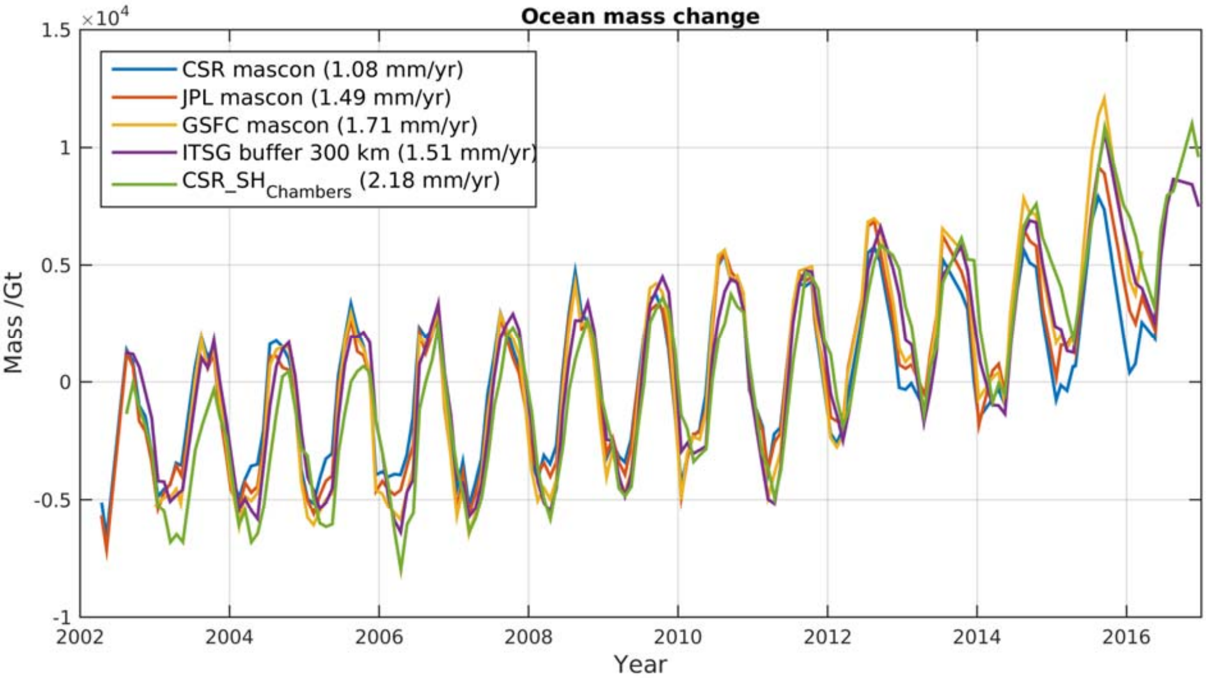

Figure 5: Time series of global integral ocean mass change. Adjusted linear trends are quoted in the legend.

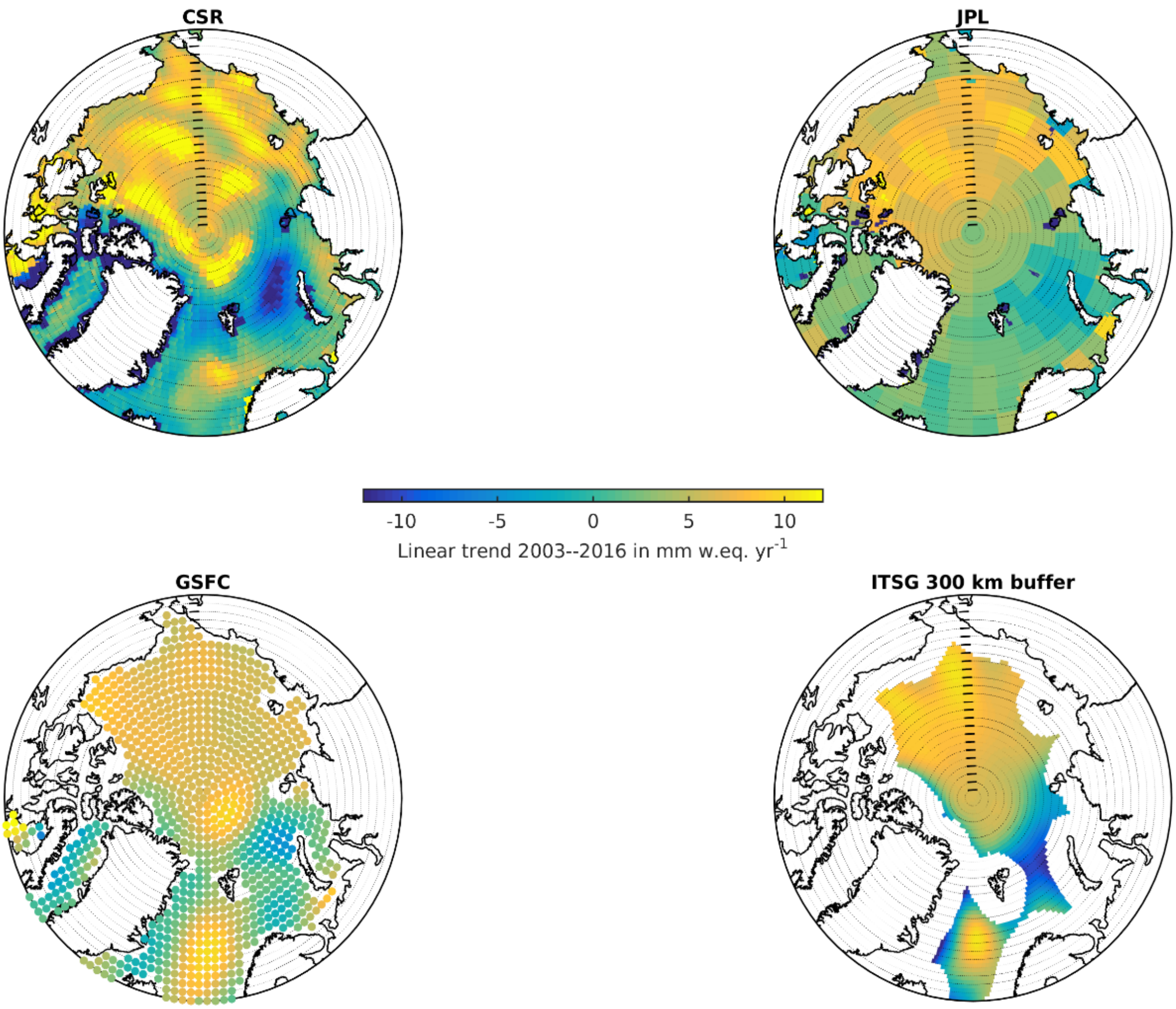

Figure 6: Linear trends of equivalent water height between 2003 and 2016 for the Arctic Ocean region. The trend was calculated like for Fig. 1. For the GSFC mascons their ocean mask was used to define the ocean area. For the other solutions, a global coastline from the Generic Mapping Tools was used here. For the ITSG dataset, an additional 300 km buffer zone was applied.

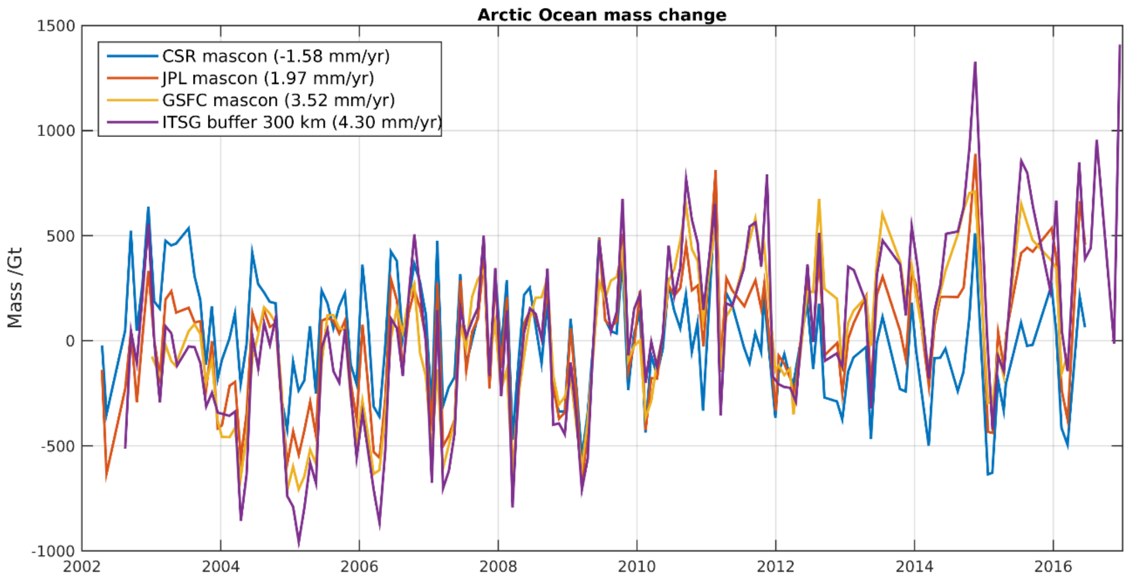

Figure 7: Time series of the Arctic Ocean (north of 66°N) integral ocean mass change. Four estimates (see legend). Adjusted linear trends are quoted in the legend.

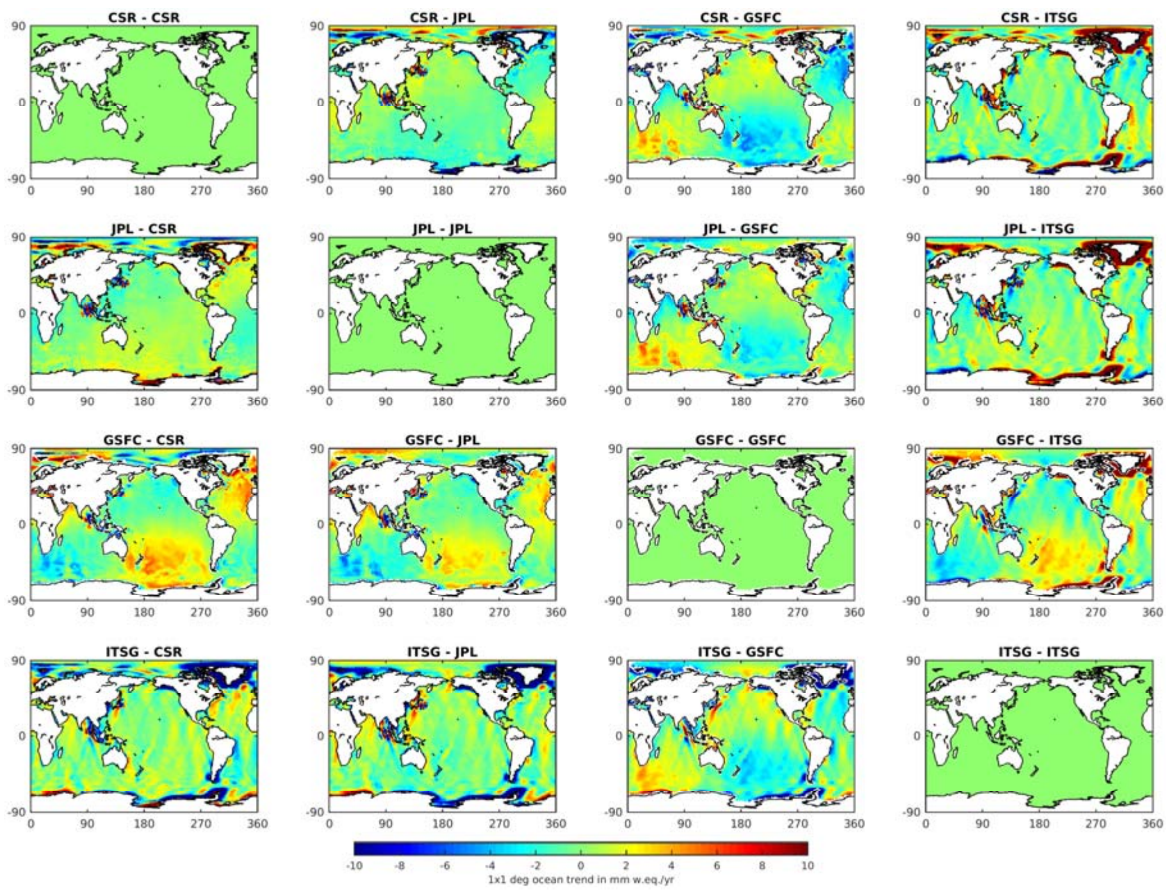

Figure 8: Ocean trend differences on a 1x1 degree grid (linear interpolation).

3.4.4. Uncertainty documentation in the data products

The data products partly contain error measures for the anomalies of the individual months. ITSG-Grace2016 solutions are provided together with full formal error variance-covariance matrices. However, the essential error sources as outlined in Section 3.4.1 must be assessed by analyses.

3.5. References

A, G., Wahr, J., and Zhong, S. (2013). Computations of the viscoelastic response of a 3-D compressible Earth to surface loading: an application to Glacial Isostatic Adjustment in Antarctica and Canada. *Geophysical Journal International*, 192(2), 557-572.

Chambers, D. P., and J. A. Bonin (2012), Evaluation of Release-05 GRACE time-variable gravity coefficients over the ocean, *Ocean Sci.*, 8, 859–868, doi:10.5194/os-8–859-2012.

Chambers, D. P., J. Wahr, M. E. Tamisiea, and R. S. Nerem (2010), Ocean mass from GRACE and glacial isostatic adjustment, *J. Geophys. Res.*, 115, B11415, doi:10.1029/2010JB007530

Cheng, M.K., B. D. Tapley, and J. C. Ries (2013), Deceleration in the Earth's oblateness, *Jour. Geophys. Res.*, V118, 1-8, doi:10.1002/jgrb.50058, 2013.

Dobslaw, H., Flechtner, F., Bergmann-Wolf, I., Dahle, C., Dill, R., Esselborn, S., ... & Thomas, M. (2013). Simulating high-frequency atmosphere-ocean mass variability for dealiasing of satellite gravity observations: AOD1B RL05. *Journal of Geophysical Research: Oceans*, 118(7), 3704-3711.

Flechtner, F., Dobslaw, H., & Fagiolini, E. (2014). AOD1B product description document for product release 05 (Rev. 4.2, May 20, 2014). Technical Note, GFZ German Research Centre for Geosciences Department, 1.

Horwath, M., & Groh, A. (2016). Evaluation of recent GRACE monthly solution series with an ice sheet perspective. *In EGU General Assembly Conference Abstracts* (Vol. 18, p. 9728). The PDF of the final poster can be downloaded from http://www.egsiem.eu/images/publication/EGU2016/horwath_egu2016_releases_b.pdf.

Johnson, G. C., and D. P. Chambers (2013), Ocean bottom pressure seasonal cycles and decadal trends from GRACE Release-05: Ocean circulation implications, *J. Geophys. Res. Oceans*, 118, 4228–4240, doi:10.1002/jgrc.20307.

Klinger, B., Mayer-Gürr, T., Behzadpour, S., Ellmer, M., Kvas, A., & Zehentner, N. (2016). The new ITSG-Grace2016 release. *Geophys. Res. Abstr.*, 18, EGU2016–11547.

Kusche, J. (2007). Approximate decorrelation and non-isotropic smoothing of time-variable GRACE-type gravity field models. *Journal of Geodesy*, 81(11), 733-749.

Kusche, J., Uebbing, B., Rietbroek, R., Shum, C. K., & Khan, Z. H. (2016). Sea level budget in the Bay of Bengal (2002–2014) from GRACE and altimetry. *Journal of Geophysical Research: Oceans*, 121, 1194–1217, doi: 10.1002/2015JC011471.

Luthcke, S. B., Sabaka, T. J., Loomis, B. D., Arendt, A. A., McCarthy, J. J., & Camp, J. (2013). Antarctica, Greenland and Gulf of Alaska land-ice evolution from an iterated GRACE global mascon solution. *J. Glac.*, 59(216), 613–631. doi:10.3189/2013JoG12J147

Mayer-Gürr, Torsten; Behzadpour, Saniya; Ellmer, Matthias; Kvas, Andreas; Klinger, Beate; Zehentner, Norbert (2016): ITSG-Grace2016 - Monthly and Daily Gravity Field Solutions from GRACE. *GFZ Data Services*. http://doi.org/10.5880/icgem.2016.007

Peltier, W. R. (2004). Global glacial isostasy and the surface of the ice-age Earth: the ICE-5G (VM2) model and GRACE. *Annu. Rev. Earth Planet. Sci.*, 32, 111-149.

Quinn, K.J, and Ponte, R.M. (2010): Uncertainty in ocean mass trends from GRACE. *Geophys J In*, 181 (2): 762-768. doi: 10.1111/j.1365-246X.2010.04508.x

Rietbroek, R, Brunnabend, S-E, Kusche, J, Schröter, J, and Dahle,C (2016):-Revisiting the contemporary sea-level budget on global and regional scales *PNAS* 2016 113 (6) 1504-1509, doi:10.1073/pnas.1519132113.

Save, H., Bettadpur, S., & Tapley, B. D. (2016). High resolution CSR GRACE RL05 mascons. *J. Geophys. Res. Solid Earth*, . doi:10.1002/2016JB013007

Swenson, S., and Wahr, J. (2006). Post-processing removal of correlated errors in GRACE data. *Geophysical Research Letters*, 33(8).

Swenson S., Chambers D., and Wahr J. (2008): Estimating geocenter variations from a combination of GRACE and ocean model output. *Journal of Geophysical Research: Solid Earth*, 113(B8).

Tamisiea, M.E. (2011): Ongoing glacial isostatic contributions to observations of sea level change. *Geophys J Int*., 186 (3): 1036-1044. doi: 10.1111/j.1365-246X.2011.05116.x

Tapley, B. D., Bettadpur, S., Watkins, M., & Reigber, C. (2004). The gravity recovery and climate experiment: Mission overview and early results. *Geophys. Res. Lett.*, 31, L09607. doi:10.1029/2004GL019920

Wahr, J., M. Molenaar, & F. Bryan (1998). Time variability of the Earth's gravity field: Hydrological and oceanic effects and their possible detection using GRACE, *J. Geophys. Res.*, 103(B12), 30205–30229, doi:10.1029/98JB02844.

Wahr, J., Nerem, R. S., & Bettadpur, S. V. (2015). The pole tide and its effect on GRACE time-variable gravity measurements: Implications for estimates of surface mass variations. *Journal of Geophysical Research: Solid Earth*, 120(6), 4597-4615.

Watkins, M. M., Wiese, D. N., Yuan, D. - N., Boening, C., & Landerer, F. W. (2015). Improved methods for observing Earth's time variable mass distribution with GRACE using spherical cap mascons: Improved Gravity Observations from GRACE. *J. Geophys. Res. Solid Earth*, 120(4), 2648–2671. doi:10.1002/2014JB011547

4. Glacier Contribution to Sea Level Change

4.1. Data Access and Requirements

The glacier evolution model used to calculate glacier mass changes and their contribution to sea level (Marzeion et al. 2012) requires (1) global glacier outlines, (2) atmospheric boundary conditions, and (3) measured mass balances (for calibration and validation) as an input. These datasets are freely available from the following sites: Glacier outlines are taken from the Randolph Glacier Inventory (RGI) version 5.0 (updated from Pfeffer et al. 2014) that provides an initial extent for each of the world's glaciers and is available from glims.org/RGI. Atmospheric boundary conditions were obtained from the CRU gridded climate data version 3.24 (updated from Harris et al. 2014) that are available from http://browse.ceda.ac.uk/browse/badc/cru/data/cru_ts/ in combination with the spatially higher resolved climatological dataset CRU CL 2.0 (updated from New et al. 2002) that can be obtained from https://crudata.uea.ac.uk/cru/data/hrg/tmc/. The model is calibrated and validated using observations of glacier mass balance from the collections of the World Glacier Monitoring Service (WGMS, 2016) that are available from wgms.ch.

4.2. Algorithms

4.2.1. Review of scientific background

The objective of model-based estimates of glacier mass change is to complement observations of glaciers with observations of the state of the atmosphere and physical understanding of glacier mass balance. While there is a growing number of glacier models being developed and used for projecting future glacier change, there is currently only one that allows to reconstruct past and reproduce current glacier change on the global scale, while also accounting for glacier geometry change (Marzeion et al. 2012). We will use this model for all calculations, as a specific aim of this project is also the globally consistent reconstruction of former glacier extents and their contribution to sea level. Special constraints such as storage of water in endorheic basins or potential future lakes forming in overdeepenings of currently still glacier covered glacier beds have to be considered separately.

4.2.2. Algorithms

The model uses observations of temperature and precipitation to estimate the glacier mass balance. Changes in glacier geometry are modeled following an area-volume-time scaling approach, enabling the model to account for various feedbacks between glacier geometry and mass balance. Glacier geometries obtained through remote sensing (from the RGI) are used to initiate the model, as well as validate results and obtain error characteristics. From the time of initialization, the model is run forward by using volume changes obtained from the mass balance module to calculate changes in glacier area, length, and terminus altitude. Glacier changes prior to the time of initialization are obtained using an iterative process: the model is also run forward during the time preceding the initialization. However, to find the correct starting conditions, the model iteratively searches for that state of the glacier at the beginning of the model run, which results in the observed state of the glacier at the time of glacier observation (i.e., at the time the glacier outlines were obtained). A detailed description of the model is found in Marzeion et al. (2012).

4.3. Product Specification

4.3.1. Product geophysical data content

Four variables are given:

1. Glacier mass change is calculated in the unit m water equivalent (w.e.) and multiplied with glacier area (in m^2) and ice density (900 kg m^{-3}) to obtain the mass of water in Gt. This is the temporally accumulated mass contribution of glaciers within each grid cell to sea level change. Mass loss of glaciers is counted positive (see Figure 9 and Figure 10). Regional or global values of glacier mass change are obtained by summing over the region of interest.
2. Glacier mass change rates are in the unit Gt/yr. This is the rate of mass contribution of glaciers within the grid cell to sea level change. Mass loss of glaciers is counted positive (see Figure 10).
3. Uncertainties of glacier mass change are originally also in the unit m w.e. (or kg m^{-2}) and are finally converted to Gt. These uncertainties are accumulated temporally forward and backward from the initialization year of each glacier, and then accumulated spatially for all glaciers contained within each grid cell. The value from 1. ± this uncertainty indicates the 5^{th} to 95^{th} percentile of the uncertainty band. Regional or global values of this uncertainty can be obtained by taking the square root of the sum of the squares of these uncertainties over the region of interest.
4. Uncertainties of glacier mass change rates are finally reported in the unit Gt/yr. The value from 2. ± this uncertainty indicates the 5th to 95th percentile of the uncertainty band. Regional or global values of this uncertainty can be obtained by taking the square root of the sum of the squares of these uncertainties over the region of interest.

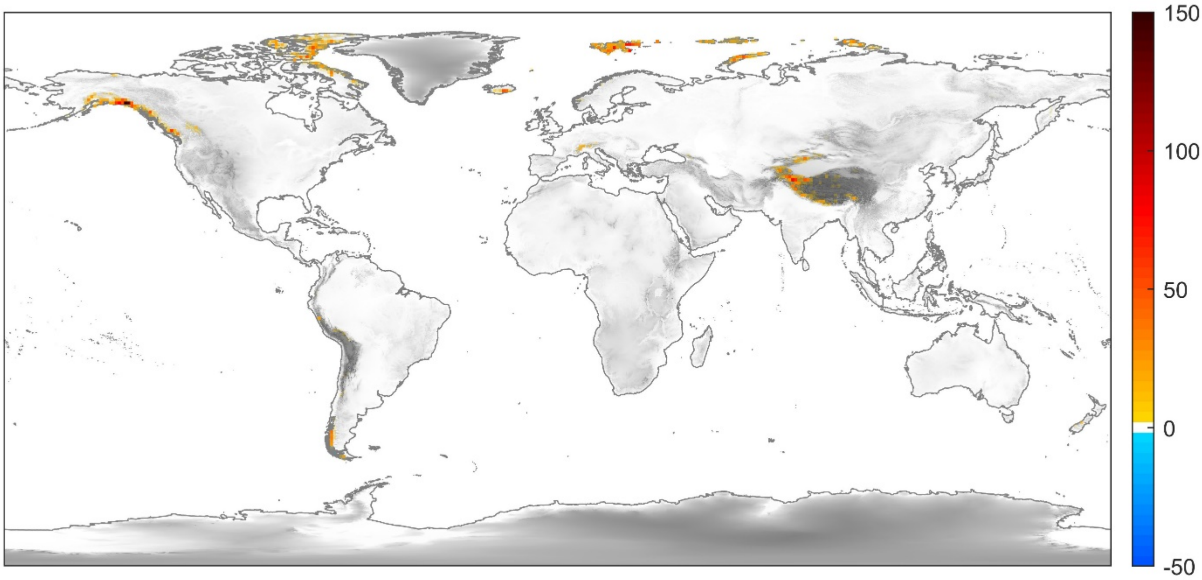

Figure 9: Spatial distribution of glacier mass loss (in Gt per grid cell) during the time 1979 to 2015.

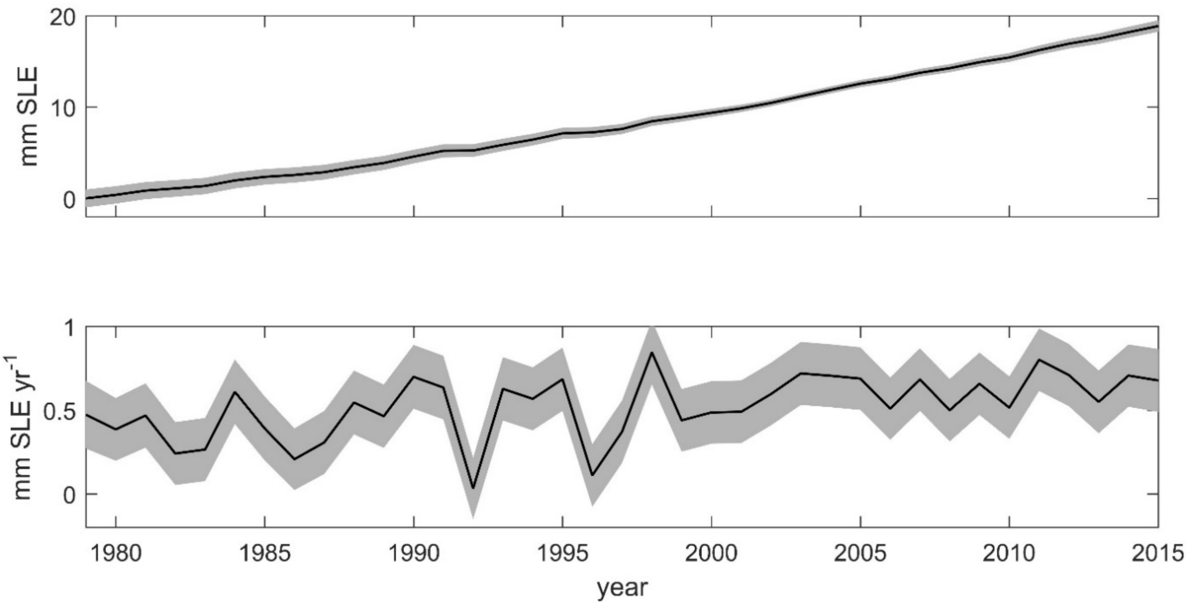

Figure 10: Spatially (and temporally, upper panel) accumulated glacier mass loss (rates, lower panel) during 1979 to 2015. Shading indicates the 5-95% confidence interval.

Data are provided with the file *glaciers_cru_324_rgi_v5.nc*

Geophysical Variable	**Name in product**	**Unit**
Glacier mass change	mass_change	Gt
Glacier mass change rate	mass_change_rate	Gt/yr
Uncertainty of glacier mass change	mass_change_uncertainty	Gt
Uncertainty of glacier mass change rates	mass_change_rate_uncertainty	Gt/yr

4.3.2. Coverage and resolution in time and space

Data coverage is global, but excluding peripheral glaciers in Greenland and Antarctica. Data are provided starting 1979 through to 2015. The resolution in space is one degree and the resolution in time is one year.

4.3.3. Product data format

Data are provided in netcdf4 format.

4.3.4. Product grid and projection

Data are provided on a rectangular grid. Latitude and longitude values of the grid correspond to the center of the grid cell. Each glacier is assigned to that grid cell that contains its center point (as given in the RGIv5.0), even if the glacier stretches across several grid cells.

4.4. Uncertainty assessment

4.4.1. Sources of error

The most relevant sources of error are:

1. uncertainty in the initialization data set (i.e., errors in glacier outlines);
2. simplification of physics in the model (concerning both the mass balance module and the simple representation of ice dynamics);
3. uncertainty in the forcing data (i.e., scarce observations of temperature and precipitation near glaciers that impact on the aggregated climate data used),
4. uncertainty in the observations of glacier mass balance used to calibrate the model;
5. uncertainty in the model calibration.

4.4.2. Methodology for uncertainty assessment

The total uncertainty of the resulting glacier mass change estimates is determined using a leave-one-glacier-out cross validation of the glacier model. In this procedure, the out-of-sample uncertainties of the model are measured by:

1. calibrating the model based on glacier observations, but withholding from the calibration all observations from one glacier;
2. running the model for that glacier and determine model error;
3. repeat the above two steps for all glaciers with available mass balance observations.

A total of 255 glaciers with 3997 observed mass balance years can currently be used in this procedure.

As uncertainties in the estimated mass balance feed back to the modeled glacier geometry, these uncertainty estimates were then propagated through the entire model chain, forward and backward in time relative to the year of model initialization. The obtained uncertainty estimates of temporally integrated glacier area and volume change were then validated once more using observations of glacier area and volume change.

4.4.3. Results of uncertainty assessment

The here provided first version of the dataset is based on Marzeion (2012) and has a mean temporal correlation between modeled and observed mass balances of individual glaciers of 0.6 with a skill score of 0.34. The mean model bias in the mass balance is indistinguishable from zero (5 mm w.e.). The mean root mean square error of modeled mass balances for individual glaciers is 736 mm w.e. The model errors are spatially and temporally uncorrelated. While the model results for any given individual glacier are therefore quite uncertain, the relative error becomes smaller for ensembles of glaciers (e.g. all glaciers within a grid cell, on a mountain range, or globally, see Figure 10).

Since errors grow forward and backward relative to the time of model initialization, and since model initialization occurs at different years for different glaciers (depending on the year the glacier geometry of observed), the uncertainties of rates of mass change are not trivially to derive from the uncertainties of accumulated glacier mass changes. Both uncertainties are given explicitly in the data product.

4.4.4. Uncertainty documentation in the data products

The delivered data file contains gridded fields of the uncertainty for both glacier mass change rates (in Gt/yr) and for temporally accumulated mass change (in Gt). See section 4.3.1.

4.5. References

Harris, I. P. D. J., Jones, P. D., Osborn, T. J., & Lister, D. H. (2014). Updated high-resolution grids of monthly climatic observations–the CRU TS3. 10 Dataset. *International Journal of Climatology*, 34(3), 623-642.

Marzeion, B., Jarosch, A. H., & Hofer, M. (2012). Past and future sea-level change from the surface mass balance of glaciers. *The Cryosphere*, 6(6), 1295.

New, M., Lister, D., Hulme, M., & Makin, I. (2002). A high-resolution data set of surface climate over global land areas. *Climate Research*, 21(1), 1-25.

Pfeffer, W. T., Arendt, A. A., Bliss, A., Bolch, T., Cogley, J. G., Gardner, A. S., ... & Miles, E. S. (2014). The Randolph Glacier Inventory: a globally complete inventory of glaciers. *Journal of Glaciology*, *60*(221), 537-552.

WGMS (2016): Fluctuations of Glaciers Database. World Glacier Monitoring Service, Zurich, Switzerland. DOI:10.5904/wgms-fog-2016-08. Online access: http://dx.doi.org/10.5904/wgms-fog-2016-08

5. Ice Sheets Contribution to Sea Level Change

5.1. Data access and requirements

Four datasets describing the mass variation and changes of the polar ice sheets are given here:

(1) Greenland Ice Sheet mass changes from GRACE

The data set described here is the time series of mass changes of the Greenland Ice Sheet derived from GRACE data. The product is publicly available as one of the ECVs of the Greenland Ice Sheet CCI, and hence is described in depth in the various documents (deliverables) of this programme. Therefore, it will not be described as thoroughly here. The summary here is based on the reference documents from the Greenland Ice Sheet CCI .

The GRACE-derived time series for Greenland is available for free download at http://products.esa-icesheets-cci.org/products/downloadlist/GMB/ (for product specifications see Sørensen L.S., et al. (2017))

At this site, two products are available; one generated by TU Dresden and one by DTU Space. The data submitted here are the ones derived by DTU Space.

GRACE data are available from different processing centres, and for the data submitted here we make use of the ITSG-Grace2016 release provided by TU Graz (www.tugraz.at/institute/ifg/downloads/gravity-field-models/itsg-grace2016), which includes spherical harmonic coefficients up to degree lmax=60.

(2) Antarctic Ice Sheet mass changes from GRACE

The data set described here is the time series of mass changes of the Antarctic Ice Sheet derived from GRACE data. The product is publicly available as one of the ECVs of the Antarctic Ice Sheet CCI, and hence is described in depth in the various documents (deliverables) of this programme. Therefore, it will not be described as thoroughly here. The relevant documents are are available at ftp://anon-ftp.ceda.ac.uk/neodc/esacci/ice_sheets_antarctica/docs/, namely

- ST-UL-ESA-AISCCI-ATBD-001_v1.0.pdf: Algorithm Theoretical Baseline Document (ATBD)
- ST-UL-ESA-AISCCI-CECR-001_v1.1.pdf: Comprehensive Error Characterisation Report (CECR)
- ST-UL-ESA-AISCCI-PSD-001_v1.1.pdf: Product Specification Document (PSD)
- ST-UL-ESA-AISCCI-PUG-001_v1.2.pdf: Product User Guide (PUG)

The datasets are available from ftp://anon-ftp.ceda.ac.uk/neodc/esacci/ice_sheets_antarctica/data/gravimetric_mass_balance/. In addition, the datasets and the documentation can be obtained at the interactive geodetic data portal of TU Dresden at https://data1.geo.tu-dresden.de/ais_gmb/index.html.

(3) Greenland Ice Sheet mass changes from altimetry

The data set described here is the mean mass loss grid for the Greenland Ice Sheet (GrIS) in the time period 2003-2009 derived from ICESat laser altimetry and snow/firn modelling. This is the data set that has been submitted to the IMBIE 2016 intercomparison exercise (except that here the full grid is provided, for IMBIE the sum over the different basins was provided). The data product is an updated version of what was published in Sørensen et al. (2011). This document explains the basic information and highlight updates, for details please refer to Sørensen et al. (2011).

The ICESat mass change data evaluation follows Sasgen et al. (2012), Sørensen et al. (2011), with an update of the ICESat data to the product release 34. In addition, the GIA- and firn-corrections have also been updated.

The mass change grid is derived from elevation changes derived from ICESat laser altimetry data release 34 available through NSIDC (http://nsidc.org/data/icesat/data_releases.html#rel34-alt).

The Firn model is forced by output data from the RCM HIRHAM5 model (Langen et al., 2015; Lucas-Picher et al., 2012).

The mass change grid data product is not currently available for download as it was specifically created for use in the IMBIE 2016 (http://imbie.org/imbie-2016/).

(4) Antarctic Ice Sheet mass changes from altimetry

The data set described here is the time series of ice mass loss for the East and West Antarctic Ice Sheet (AIS) the period time period 1992-2016 derived from radar altimetry and a time evolving ice density mask. This is the data set that has been submitted to the IMBIE 2016 intercomparison exercise. Data from the 2010-2016 is published in McMillan et al., (2014), and the full 25 year time series is will be submitted for publication within the coming month (Shepherd et al., TBD). This document explains the basic information about the dataset, for details of the plane fit method, please refer to (McMillan et al., 2014).

The mass change time series is derived from surface elevation change generated by processing Level 2 elevation measurements provided by ESA, and acquired by multiple radar altimetry satellite missions, ERS-1, ERS-2, ENVISAT and CryoSat-2. The lateral limit used for both the Greenland and Antarctic ice sheet CCI can be found at the following link (http://imbie.org/imbie-2016/), and this has been provided to the Glaciers and Ice Caps CCI project team.

A complimentary gridded data product is also available to show the spatially variable pattern of ice loss and can be added at a later stage of the project if necessary.

5.2. Algorithms

5.2.1. Review of scientific background

Ice Sheet mass changes from GRACE

The GRACE mission has two identical spacecrafts flying about 220 km apart in a near-polar orbit originally at 500 km above the Earth. GRACE maps the Earth's gravity fields by making accurate measurements of the distance between the two satellites, using GPS and a microwave ranging system. GRACE-derived solutions of the Earth's time variable gravity field are available from different processing facilities like CSR, GFZ or JPL. With a typical temporal resolution of one month, GRACE Level-2 products allow the investigation of seasonal and inter-annual variations in addition to long-term changes (Horwath et al., 2012). A comprehensive review of scientific background is found in Khvorostovsky, et al. (2016).

Greenland Ice Sheet mass changes from altimetry

Satellite laser altimetry is used to derive elevation changes of the GrIS for the given time period. The elevation changes are interpolated to cover the entire ice sheet. The elevation changes are corrected for any elevation change signal that is not associated with ice mass loss (GIA, elastic uplift and changes in firn compaction), and finally converted into grid point mass changes using assumptions on ice/snow densities (Figure 11). This procedure is described in detail in Sørensen et al., 2011.

Antarctic Ice Sheet mass changes from altimetry

Satellite laser altimetry is used to derive elevation changes of the AIS for the full 25 year epoch over which satellite radar altimetry measurements are available. The elevation changes are interpolated to cover the entire ice sheet. The elevation changes are corrected for any elevation change signal that is not associated with ice mass loss (GIA, elastic uplift and changes in firn compaction), and finally converted into grid point mass changes using assumptions on ice/snow densities. This procedure is described in detail in Sørensen et al., 2011.

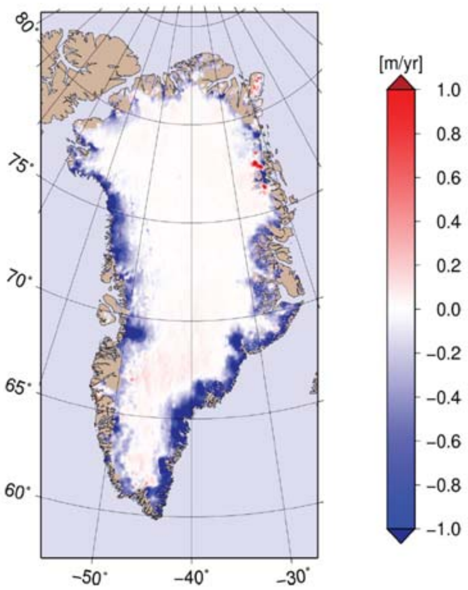

Figure 11: Point mass changes from Sørensen et al., 2011. Given as water equivalent per year.

5.2.2. Algorithms

Greenland Ice Sheet mass changes from GRACE

Methods used for the inference of ice sheet mass changes from GRACE data is divided into two main groups:

1. Inversion approaches
2. Regional integration approaches

The mass inversion method has been adopted for the GMB product generation, within the GIS CCI.

A detailed description of the method and associated algorithms is provided in Sect. 6.3.1 of Khvorostovsky, et al. (2016).

Antarctic Ice Sheet mass changes from GRACE

The Antarctic Ice Sheet GMB products are derived from the spherical harmonic monthly solution series by ITSG-Grace2016 by TU Graz (Klinger et al. 2016; Mayer-Gürr et al. 2016) following a regional integration approach with tailored integration kernels that account for both the GRACE error structure and the information on different signal variance levels on the ice sheet and on the ocean (Horwath and Groh 2016).

Greenland Ice Sheet mass changes from altimetry

Elevation change method

Several methods for deriving elevation changes from repeat laser altimetry exist. Here, we have used M3 of Sørensen et al., 2011, which was also used in Sasgen et al., 2012.

Correction for Glacial Isostatic Adjustment

The ICE-6g (Peltier et al., 2015) rate of radial displacement (UP) have been interpolated from the 0.2°x0.2° grid posting given in the drad.12mgrid.nc dataset available at http://www.atmosp.physics.utoronto.ca/~peltier/data.php.

Correction for elastic uplift

The instantaneous elastic vertical displacement is applied following Sørensen et al. (2011) is obtained from a suitably modified version of the code SELEN 2.9 (Nielsen et al., 2014; Spada and Stocchi, 2007).

Correction for changes in air content in the firn:

The firn model follows Simonsen et al. (2013), which include a parameterization of melt water retention. The firn model is forced by the HIRHAM5 regional climate model (Langen et al., 2015; Lucas-Picher et al., 2012), which have been updated with a new and improved surface scheme compared to the version used in Nielsen et al. (2014) (Sasgen et al., 2012; Sørensen et al., 2011).

Antarctic Ice Sheet mass changes from altimetry

Elevation change method

Several methods for deriving elevation changes from repeat laser altimetry exist. Here, we have employed the plane fit method (McMillan et al., 2014). The plane fit method (McMillan, *et al.*, 2014) is an adaption of the along track method which can be applied to satellites which operate in both short 27-35 day orbit repeat periods (such as the main operational periods of Envisat, ERS-1,2 and Sentinel-3A,B) and long 369 day repeat periods where measurements do not exactly repeat within monthly time scales such as CryoSat-2.

The plane fit method grids both ascending and descending measurements in a regular polar stereographic grid instead of gridding separately along track. It derives a surface elevation change estimate at the centre of each grid cell by applying a surface model to the measurements within that cell and has been shown in the CCI round robin experiments to perform as well or better than other along track methods for all missions (except Envisat's drifting phase from Oct 2010- Apr 2012, where special techniques are required for all methods) and hence is the primary along track method chosen for the Antarctic CCI. Another advantage of the plane fit method is that SEC results are produced on the same grid as the SEC output product and hence do not require re-gridding which can introduce an additional error and reduce accuracy.

Correction for Glacial Isostatic Adjustment

A post-glacial rebound (PGR) correction was applied to all the residual heights in each selected cell. The correction used was the IJ05_R2 correction, from Ivins and James et al, 2013.

Pole Hole Filling

In the chosen region and epoch grid, cells within the pole hole were filled using the mean of all the observed cells in that region and epoch that were in the latitude band 80^0S to 81^0S.

Derivation of Height Time Series

Time series calculations used the dz and dt values retained after the model-fitting stage, which were only calculated for grid cells that were observed by satellite. Time series can be calculated over any region. For this study the East and West Antarctic Ice Sheets as defined by Zwally et al. (2012) were used. In each case, unobserved grid cells had to be filled.

Inter-Mission Cross Calibration

The previous calculations produced a time series of changes in height per mission. To produce a continuous dataset, biases had to be added between missions. The biasing method used is applied to each grid cell individually, which is known as pixel cross-calibration. In each case, the biasing aimed to bring ERS1, ERS2 and CryoSat-2 data onto the same baseline as the Envisat data.

Conversion from Volume to Mass

As radar altimeters penetrate some (unknown) depth into the snow surface, direct application of a firn correction to the elevation change measurement, and then derivation of mass at the density of ice from the residual signal, has known issues in Antarctica. Therefore we use a time-evolving density mask to delimit the region where we convert volume to mass at the density of snow ($350 kg/m^3$) and ice ($917 kg/m^3$). To derive mass change, grid cells are identified as containing changing amounts of either snow or ice, using a time-dependent density mask. In this study the density mask was derived from the pixel cross-calibrated timeseries and the Berkeley Ice Sheet Initiative for Climate Extremes (BISICLES) ice velocity map (Cornford et al, 2013).

5.3. Product Specification

5.3.1. Product geophysical data content

Greenland Ice Sheet mass changes from GRACE

The geophysical data content is a time series of the ice mass changes. Both entire-ice sheet (Figure 12) and basin estimates are provided.

The total ice sheet time series is constructed so that the estimate also includes the signal from outlying Glaciers and ice caps, while the individual basin estimates are derived in a way that aims at leaving those out of the solution. Therefore, there is a difference between the mass balance derived from the total time series and the sum of the individual basins. For more information, see Khvorostovsky, et al. (2016).

The drainage basins used are an aggregation of those described by Zwally et al. (2012). Figure 13 below shows the outline of the basins.

For further information on how Ice sheet and the surrounding glaciers and ice caps are separated see Khvorostovsky et al. (2016).

The temporal coverage is constrained by the data availability, and is continuously extended as data become available. The temporal resolution is monthly estimates (some months are missing due to missing data.)

Antarctic Ice Sheet mass changes from GRACE

Mass change time series are provided for a number of drainage basins, based on the boundary definitions by Zwally et al. (2012). They describe the evolution of ice mass relative to a modelled reference value. This reference value is defined to be the GRACE-derived mass as of

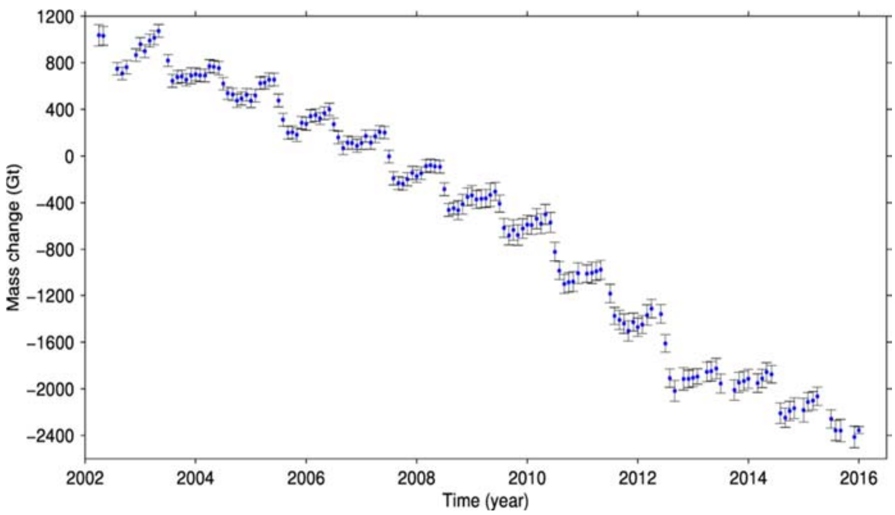

Figure 12: Mass change time series from Greenland Ice sheet derived by DTU Space

2009-01-01. Respective time series are also derived for the total areas of the West Antarctic Ice Sheet, the East Antarctic Ice Sheet, the Antarctic Peninsula and the Antarctic Ice Sheet (AIS) as a whole.

The gridded changes are given in millimetre of equivalent water height (mm w.eq., or kg/m^2). The applied algorithm is consistent with the one used for the GMB Basin Product.

Greenland Ice Sheet mass changes from altimetry

The geophysical data content is a grid of mass changes. The file submitted for the SLBC project is named „SLBC_ICESat_mass_2003_2009.txt“

The mass change grid product represents the mean mass change for the period with useful laser altimetry data: Oct 2003–Oct 2009 (2003.75 - 2009.83).

The file contains point location, mass change, error on mass (provided as the standard deviation), area of the grid cell over which the mass change is calculated.

The sum of the mass changes over the whole grid (Greenland ice sheet + outer glaciers and ice caps) is -238.5 Gt/yr (cf. Table 3).

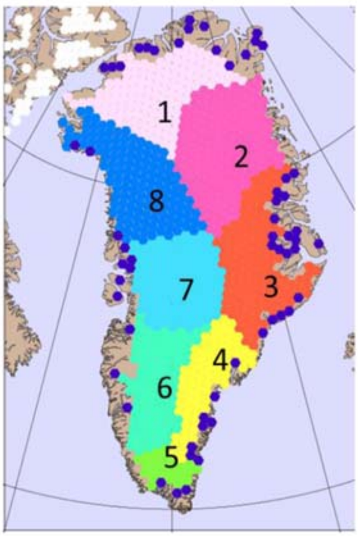

Figure 13: Eight main Greenland Ice Sheet basins (Zwally et al., 2012) colour-coded. Glaciers and ice caps marked with dark blue.

Table 3: The summed mass balance

	Full grid	Zwally et al., 2012 basin outlines		
	GrIS + Outer Glaciers and Ice Caps	GrIS	Above 1500 m	Below 1500 m
Total mass balance [Gt/yr]	-238.5	-204.9	-62.1	-142.7
Uncertainty [+/- Gt/yr]	28	28	15	18

Antarctic Ice Sheet mass changes from altimetry

The geophysical data content is a time series of mass change, for the full 25 year period over which radar altimetry data is available (Figure 14).

The mass change time series product represents the cumulative mass change for the period with useful radar altimetry data: March 1992–March 2016 (1992.3 - 2016.3).

The file contains time, mass change, and error on mass for the East and West Antarctic ice sheet.

The total cumulative mass change for West Antarctica (WAIS) is -1148 Gt, and -143 Gt for East Antarctica (EAIS) (Table 4).

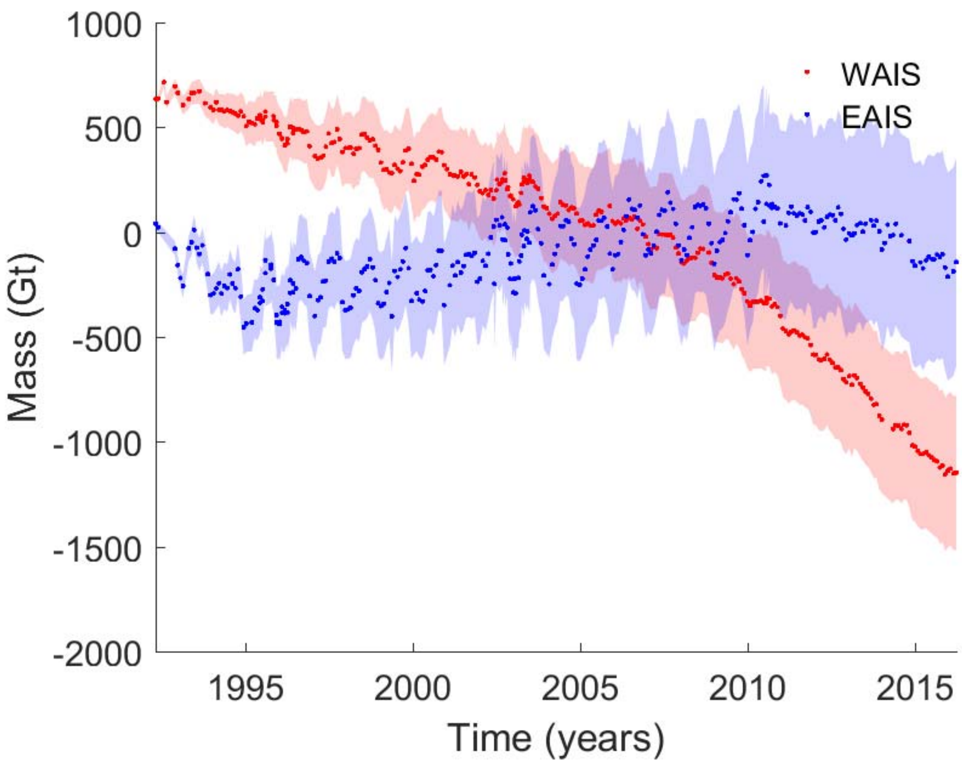

Figure 14: Cumulative Mass changes from East and West Antarctica (Shepherd et al., TBD).

Table 4: The summed mass balance

	Zwally et al., 2012 basin outlines	
	WAIS	EAIS
Cumulative mass balance [Gt]	-1148	-143

5.3.2. Product data format

Greenland Ice Sheet mass changes from GRACE

The mass change time series are provided for both the entire ice sheet and for drainage each basin (detailed information is found in Khvorostovsky et al. (2016)).

The time series are given in a simple ASCII format of the following form:

Time [decimal year]	Mass change [Gt]	Error on mass change [Gt]

Where the mass change is the mass anomaly in Gt (relative to a chosen zero level) with the associated errors (see Forsberg et al., 2103). One file for each basin and one for entire GIS is provided, with their file names indicating content:

GIS00_grace.dat: Mass change time series for entire GIS
GIS01_grace.dat: Mass change time series for basin 1
GIS02_grace.dat: Mass change time series for basin 2
GIS03_grace.dat: Mass change time series for basin 3
GIS04_grace.dat: Mass change time series for basin 4
GIS05_grace.dat: Mass change time series for basin 5
GIS06_grace.dat: Mass change time series for basin 6
GIS07_grace.dat: Mass change time series for basin 7
GIS08_grace.dat: Mass change time series for basin 8

Antarctic Ice Sheet mass changes from GRACE

The GMB gridded product is available in the following three file formats:

1. NetCDF (*AIS_GMB_grid.nc*)
2. GeoTIFF (*AIS_GMB_grid.tif*)
3. ASCII (*AIS_GMB_grid.dat*)

The NetCDF-4 classic file follows the Climate and Forecast (CF) conventions in version 1.6. Changes in ice mass are stored in the NetCDF variable *dm* [kg/m^2]. Beside the projected x- and y-coordinates of the grid cell centres, corresponding ellipsoidal latitudes (*lat*) and longitudes (*lon*) are also given. In addition, each grid cell's area (*area*) on the ellipsoid is provided. Times are indicated in two different formats: modified Julian date (*time*) and decimal years (*time_dec*). Additional information on the product and the generating institution are stored in the global attributes.

Content of *AIS_GMB_grid.nc*

Geophysical Variable	Name in product	Unit
x-coordinate, y-coordinate	x, y	m
Modified Julian Date	time	days
Decimal year	time_dec	year
Longitude, Latitude	lon, lat	degrees_east, degrees_north
Change in ice mass	dm	kg/m^2
Grid cell area on the ellipsoid	area	m^2
Projection Type (Name of projection and parameters used)	crs	-

The file *AIS_GMB_grid.dat* contains time series of mass change per grid point

x	y	lat	lon	area	dm1 at time1, dm2 at time2, dm3 at time 3, ...
[m]	[m]	[°]	[°]	[m^2]	[kg/m^2]

In addition, file *AIS_GMB_basin.dat* gives GRACE-derived time series of basin-averaged Antarctic ice mass changes in the form

time	time	dm basin1 [kg], sigma dm basin1 [kg], ...
[decimal year]	[modified julian data]	

The mass balance (mb) linear trend inferred from GRACE-derived time series of basin-averaged Antarctic ice mass changes is provided with the file *AIS_GMB_trend.dat*.

basin	mb	sigma mb	GIA	area
	[kg/yr]	[kg/yr]	[kg/yr]	[m^2]

Greenland Ice Sheet mass changes from altimetry

The mass change grid (provided in file SLBC_ICEsat_mass_change_2003_2009.txt) is given in a simple ASCII format of the following form:

Latitude [degree]	Longitude [degree]	Mass change [kg/year]	std.dev of mass [kg]	area [km^2]

Antarctic Ice Sheet mass changes from altimetry

The mass change time series (provided in file *SLBC_RA_*AIS_mass_1992_2016.csv*) is given in two simple comma separated text format of the following form:

time [date]	cumulative mass [Gt]	error estimate [Gt]

5.3.3. Product grid and projection

Greenland Ice Sheet mass changes from GRACE

The GMB data are simply mass change time series of Ice sheet-wide, and basin scale.

Antarctic Ice Sheet mass changes from GRACE

For the map projection utilized for the GMB gridded product a polar stereographic projection with reference latitude at 71°S, reference meridian at 0°, and based on the ellipsoid WGS84 (EPSG3031) is used.

Greenland Ice Sheet mass changes from altimetry

The mass changes are provided on the ice covered areas of Greenland, as defined by the land cover type grid available here: http://websrv.cs.umt.edu/isis/index.php/Present_Day_Greenland. The grid resolution is 5 km.

Antarctic Ice Sheet mass changes from altimetry

A gridded data product had not been provided yet, however as stated earlier in this document, it can be made available if the information is required for the project.

Uncertainty Assessment

5.3.4. Sources of error

Ice Sheet mass changes from GRACE

The error characterization of the GRACE product is provided in detail in Forsberg et al., 2103. Errors in GRACE-derived mass changes have several origins. The three major contributions arise from:

1. GRACE errors in the monthly solutions.
2. Leakage errors due to the limited spatial resolution achieved by GRACE.
3. Errors in models used to reduce superimposed mass signals.

Greenland Ice Sheet mass changes from altimetry

The sources of errors are

1. Uncertainty in the interpolation of elevation change point estimates into volume change
2. error in the firn compaction
3. error in bedrock movement
4. error from neglecting basal melt and possible ice build-up above the Equilibrium Line Altitude (ELA).

Antarctic Ice Sheet mass changes from altimetry

There are error sources and uncertainties originating from the data themselves that will influence the radar measured elevations and hence the estimated surface elevation change. Among these are:

1. uncertainties in the satellite orbit and attitude
2. atmosphere propagation corrections
3. solid earth tides and ocean tide to remove the effect of local tidal distortion to the Earth's crust
4. Uncertainty in the interpolation of elevation change point estimates into volume change
5. Interpolation across data gaps

While the error budget is somewhat affected by all these sources of error, it is dominated by the uncertainty related to the surface elevation change derivation and interpolation errors.

5.3.5. Methodology for uncertainty assessment

Greenland Ice Sheet mass changes from GRACE

We derive the uncertainties which are related to the data errors provided directly with the GRACE monthly models by using a Monte-Carlo-like approach in which 200 simulations are performed. The simulations are created from Stokes coefficients drawn from normal distributions with zero mean, and the standard deviation provided with the GRACE level-2 data.

In order to give an estimate at basin scale of the effect of the outer glaciers leakage effect, we compute two solutions which represent an upper and lower bound for the mass loss and find that this leakage error is between 4% and 10% of the mass trend.

The GIA error is meaningful only for the linear trends in mass changes and for the whole Greenland we use the value in Barletta et al. (2013) (Table 5). For our best value we chose to use the A et al. (2013) model which is an ICE5g-VM2 compressible model with rotational feedback. This contribution for Greenland is -5.4 Gt/yr and the uncertainty is up to +/- 7.2 Gt/yr.

The results of a thorough (mass trend) uncertainty investigation (Forsberg et al., 2103) revealed the numbers provided in Table 5 below. The error source, estimation procedure and expected range in trend values are provided.

Antarctic Ice Sheet mass changes from GRACE

The uncertainty assessment is described in detail in the Antarctic_Ice_Sheet_cci Comprehensive Error Characterisation Report (Nagler et al. 2016). Table 6 summarizes the uncertainty assessment for the entire Antarctic Ice Sheet.

Table 5: Sources and ranges of errors in GIS mass variation estimation

Error source	Estimation procedure	Expected range
GRACE solutions	Propagation of the scaled standard deviation	3.2Gt/yr
GIA model	Intercomparison of different models	7.2Gt/yr
Leakage	Analysis of use of different SA	3.2Gt/yr
Degree one	Intercomparison of different degree one time series	3 Gt/yr
Total	Individual components summed in quadrature	9Gt/yr

Table 6: Error components contributing to the overall error budget of the final GMB products for the entire AIS.

Error source	Estimation procedure	Range
Basin averaged mass change time series		
GRACE solutions	Scaled rms of the error noise, derived from the GRACE time series	68 Gt
Total		**68 Gt**
Mass balance estimates per basin		
GRACE solutions	Propagation of the scaled error rms	2 Gt/yr
GIA model	Intercomparison of different models	32 Gt/yr
Leakage AIS	Analysis of dominant patterns of dynamic mass changes	6 Gt/yr
Leakage non-AIS	Analysis of a global trend pattern (excluding AIS) derived from GRACE	1 Gt/yr
Degree one	Intercomparison of different degree one time series	13 Gt/yr
C20	Intercomparison of different C20 time series	4 Gt/yr
Total	Individual components summed in quadrature	35 Gt/yr

Greenland Ice Sheet mass changes from altimetry

Following the error sources above the uncertainty assigned for each of these four sources are:

Ad 1) The uncertainty of the ice volume change due to interpolation between the elevation changes along each satellite tracks, is estimated by applying a bootstrapping method. In the bootstrapping approach 1000 volume change estimates are derived using a randomly chosen subset of the satellite tracks, yielding a distribution of volume changes.

Ad 2) The uncertainty in the firn compaction model applied is assumed to be 20% of the estimated correction (rate of change of firn air content) applied. This is a conservative estimate of the uncertainty.

Ad 3) The uncertainty in the bedrock movements beneath the ice sheet is derived from predicting the regional elastic bedrock movement using a model developed by Giorgio Spada (University of Urbino). The uncertainty is proportional to the uncertainty of the regional ice mass change.

Ad 4) The uncertainty of neglecting basal melt was determined by assigning a Greenland-wide average melt rate of 1 mm/year. Such a melt rate corresponds to 0.9 Gt/year above the ELA. An ice sheet model has been used to evaluate the uncertainty of neglecting ice dynamics, which corresponds to 14 Gt/year

A detailed description of the error calculation is provided in Sørensen et al. (2011).

Antarctic Ice Sheet mass changes from altimetry

Surface elevation change errors in the elevation time series are calculated using the root mean square of the departure from the modelled trend.

5.3.6. Uncertainty documentation in the data products

Greenland Ice Sheet mass changes from GRACE

Monthly mass change time series per basin will be provided with an average monthly error estimate, see Figure 12.

Antarctic Ice Sheet mass changes from GRACE

Uncertainties of monthly values for the basin products are part of the products.

Uncertainties of linear trends are given in the Comprehensive Error Characterisation Report (Nagler et al. 2016) – see Table 6.

Greenland Ice Sheet mass changes from ICESat laser altimetry

The uncertainty is provided in the data product (column 4) as the standard deviation of the mass change as predicted by the bootstrapping approach (cf. Table 3).

Antarctic Ice Sheet mass changes from ICESat laser altimetry

The uncertainty is provided in the data product (column 3).

5.4. References

A, G., Wahr, J., and Zhong, S. (2013). Computations of the viscoelastic response of a 3-D compressible Earth to surface loading: an application to Glacial Isostatic Adjustment in Antarctica and Canada. *Geophysical Journal International*, 192(2), 557-572.

Barletta, V. R., Sørensen, L. S., and Forsberg, R. (2013). Scatter of mass changes estimates at basin scale for Greenland and Antarctica. *The Cryosphere*, 7(5), 1411–1432.

Cornford et al, 2013, Adaptive mesh, finite volume modelling of marine ice sheets, *Journal of Computational Physics*, 232(1):529-549.

Forsberg, R., L. Sørensen, et al. (2013): Comprehensive Error Characterisation Report for the Ice_Sheets_cci project of ESA's Climate Change Initiative, version 1.2, 06 June 2013.

Horwath, M., and Groh, A. (2016): The GRACE mass change estimators developed for ESA's CCI ice sheet mass balance products. *Proc. GRACE Science Team Meeting 2016*, Potsdam, 5-7 November 2016. http://www.gfz-potsdam.de/en/section/global-geomonitoring-and-gravity-field/topics/development-operation-and-analysis-of-gravity-field-satellite-missions/grace/gstm/gstm-2016/proceedings/.

Horwath, M., Tranchant, J.-B., van den Broeke, M., Legrésy, B. (2012) Evaluation of GRACE monthly solutions of Release 5 versus Release 4, with an ice sheet perspective. *Proc. GRACE Science Team Meeting*, September 2012, Potsdam, Germany.

Ivins E., James T., Wahr J., Schrama E., Landerer F., and Simon K. (2013): Antarctic contribution to sea level rise observed by GRACE with improved GIA correction. *J. Geophys. Res.: Solid Earth*, 118(6), 3126-3141.

Khvorostovsky, et al. (2016), Algorithm Theoretical Baseline Document (ATBD) for the Greenland_Ice_Sheet_cci project of ESA's Climate Change Initiative, version 3.1 (ST-DTU-ESA-GISCCI-ATBD-001), 09 Sep 2016.

Klinger, B., Mayer-Gürr, T., Behzadpour, S., Ellmer, M., Kvas, A., & Zehentner, N. (2016). The new ITSG-Grace2016 release. *Geophys. Res. Abstr.*, 18, EGU2016–11547.

Kusche, J. (2007). Approximate decorrelation and non-isotropic smoothing of time-variable GRACE-type gravity field models. *Journal of Geodesy*, 81(11), 733-749.

Kusche, J., Uebbing, B., Rietbroek, R., Shum, C. K., & Khan, Z. H. (2016). Sea level budget in the Bay of Bengal (2002–2014) from GRACE and altimetry. *Journal of Geophysical Research: Oceans*, 121, 1194–1217, doi: 10.1002/2015JC011471.

Luthcke, S. B., Sabaka, T. J., Loomis, B. D., Arendt, A. A., McCarthy, J. J., & Camp, J. (2013). Antarctica, Greenland and Gulf of Alaska land-ice evolution from an iterated GRACE global mascon solution. *J. Glac.*, 59(216), 613–631. doi:10.3189/2013JoG12J147

Mayer-Gürr, Torsten; Behzadpour, Saniya; Ellmer, Matthias; Kvas, Andreas; Klinger, Beate; Zehentner, Norbert (2016): ITSG-Grace2016 - Monthly and Daily Gravity Field Solutions from GRACE. *GFZ Data Services*. http://doi.org/10.5880/icgem.2016.007

Langen, P. L., Mottram, R. H., Christensen, J. H., Boberg, F., Rodehacke, C. B., Stendel, M., ... Cappelen, J. (2015). Quantifying energy and mass fluxes controlling Godthåbsfjord freshwater input in a 5 km simulation (1991-2012). *J. of Climate*. http://doi.org/10.1175/JCLI-D-14-00271.1

Lucas-Picher, P., Wulff-Nielsen, M., Christensen, J. H., Adalgeirsdóttir, G., Mottram, R. H., & Simonsen, S. B. (2012). Very high resolution regional climate model simulations over Greenland: Identifying added value. *Journal of Geophysical Research*, *117*(D), 2108. Retrieved from http://adsabs.harvard.edu/cgi-bin/nph-data_query?bibcode=2012JGRD..11702108L&link_type=ABSTRACT

McMillan, M., Shepherd, A., Sundal, A., Briggs, K., Muir, A., Ridout, A., HOgg, A., and Wingham, D. (2014). Increased ice losses from Antarctica detected by CryoSat-2. *Geophys. Res. Lett.*, 41(11), 3899-3905.

Nagler, T., et al. (2016): *Comprehensive Error Characterisation Report (CECR)*. Antarctic_Ice_Sheet_cci project, ESA's Climate Change Initiative, version 1.1, 01 May 2016, Available from: http://www.esa-icesheets-antarctica-cci.org/.

Nielsen, K., Sørensen, S. L. S., Khan, S. A., Spada, G., Simonsen, S. B., & Forsberg, R. (2014). Towards constraining glacial isostatic adjustment in Greenland by GPS observations. *International Association of Geodesy Symposia*, 1–7. JOUR. http://doi.org/10.1007/978-3-642-37222-3_43

Peltier, W. R., Argus, D. F., and Drummond, R. (2015). Space geodesy constrains ice age terminal deglaciation: The global ICE-6G_C (VM5a)model. *Journal of Geophysical Research (Solid Earth)*, *120*, 450–487. http://doi.org/10.1002/2014JB011176.Received

Sasgen, I., van den Broeke, M. R., Bamber, J. L., Rignot, E., Sørensen, S. L. S., Wouters, B., ... Sørensen, L. S. (2012). Timing and origin of recent regional ice-mass loss in Greenland. *Earth and Planetary Science Letters*, 333, 293–303. JOUR. http://doi.org/10.1016/j.epsl.2012.03.033

Simonsen, S. B., Stenseng, L., Adalgeirsdóttir, G., Fausto, R. S., Hvidberg, C. ~S., & Lucas-Picher, P. (2013). Assessing a multilayered dynamic firn-compaction model for Greenland with ASIRAS radar measurements. *Journal of Glaciology*, 59(215), 545–558.

Sørensen L.S., et al. (2017), Product Specification Document (PSD) for the Greenland_Ice_Sheet_cci project of ESA's Climate Change Initiative, version 2.3 (ST-DTU-ESA-GISCCI-PSD-001), 20 March 2017.

Sørensen, L. S., Simonsen, S. B., Nielsen, K., Lucas-Picher, P., Spada, G., Adalgeirsdóttir, G., ... Hvidberg, C. S. (2011). Mass balance of the Greenland ice sheet (2003-2008) from ICESat data - the impact of interpolation, sampling and firn density. *The Cryosphere*, *5*(1), 173–186. http://doi.org/10.5194/tc-5-173-2011

Spada, G. A., and Stocchi, P. (2007). SELEN : A Fortran 90 program for solving the "' sea-level equation .'" Computers & Geosciences, 33, 538–562. http://doi.org/10.1016/j.cageo.2006.08.006

Zwally, H. Jay, Mario B. Giovinetto, Matthew A. Beckley, and Jack L. Saba (2012): Antarctic and Greenland Drainage Systems, GSFC Cryospheric Sciences Laboratory, at http://icesat4.gsfc.nasa.gov/cryo_data/ant_grn_drainage_systems.php.

6. Total Land Water Storage Change

Variations in land water storage on multiple time scales have an impact on water exchange between land, atmosphere and ocean, ultimately affecting global ocean mass and sea level variations. They are affected by human actions that may lead to long-term trends of land water mass. Groundwater depletion, for example, decreases land water storage and increases ocean mass (Wada et al. 2012), while impoundment of water in new reservoirs retains land water (Chao et al. 2008).

6.1. Data Access and Requirements

Global and gridded time series of total (land) water storage (TWS) were obtained with the global hydrological model WaterGAP 2.2b standard, which is currently applied and developed at the Institute of Physical Geography of the University of Frankfurt. This model version is only slightly modified as compared to the model versions described in Döll et al. (2014a; 2014b) and Müller Schmied et al. (2014; 2016b).

6.2. Algorithms

6.2.1. Review of scientific background

WaterGAP consists of the WaterGAP Global Hydrology Model (WGHM) and of a number of submodels for computing human water use (Figure 15). The global water use models compute water withdrawal and water consumption for five sectors (irrigation, livestock farming, domestic use, manufacturing industries and cooling of thermal power plants). The submodel GWSWUSE distinguishes the source of abstracted water and computes net abstractions (abstractions minus return flow) from groundwater and from surface water. These net abstractions are input to WGHM.

WGHM represents the transport of water on continents as a series of different water storage compartments that are interconnected by water flows (Figure 16). The canopy, soil, snow, groundwater and surface water bodies (wetlands, lakes, rivers and reservoirs) compartments are included, whereas glaciers are not represented. Water exchanges between the compartments are computed at grid cell level. “Global” lakes and wetlands are distinguished from “local” ones by the fact that they are recharged not only by the cell runoff but also by the streamflow from upstream cells. Total grid cell runoff as computed by vertical water balance is partitioned between fast surface and subsurface runoff R_s and groundwater recharge R_g. Both runoff components are routed to the river storage compartment of the grid cell and are transported as streamflow to the downstream grid cell (Figure 16). At the global scale, river discharge is laterally routed through the stream network derived from the global drainage direction map DDM30 (Döll and Lehner 2002) until it reaches the ocean or an inland sink.

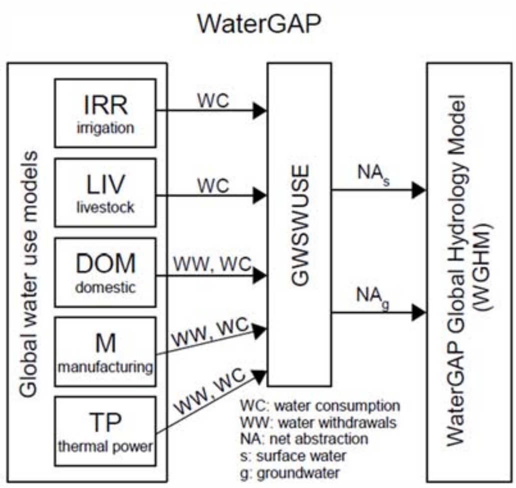

Figure 15: Schematic of WaterGAP 2.2. The output of five water use models is translated into net abstractions from groundwater NA_g and surface water NA_s by the submodel GWSWUSE, which allows computing the impact of human water use on water flows and storages by WGHM. For details see Döll et al. (2012).

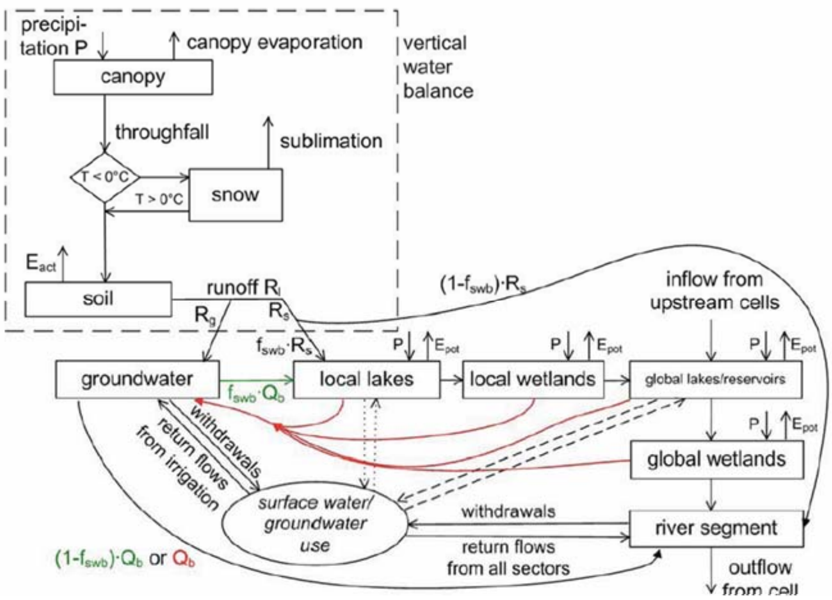

Figure 16: Schematic of water storage compartments (boxes) and flows (arrows) within each 0.5°x0.5° grid cell of WGHM, including the simulation of water use impacts on water storage in groundwater and surface water. For details see Döll et al. (2014b).

WaterGAP is calibrated against observations of mean annual river discharge at 1319 gauging stations, and the adjusted calibration factor is regionalized to grid cells outside the calibration basins (see Appendix B of Müller Schmied et al. 2014).

6.2.2. Algorithms

Considering the large amount of algorithms used within WaterGAP, this subsection will be constrained to the current state of the algorithms that we foresee to improve in the frame of the project[1].

Reservoir storage. The reservoir operation algorithm of Hanasaki et al. (2006), distinguishing irrigation and non-irrigation reservoirs and considering 1109 reservoirs, was implemented and improved by Döll et al. (2009) and subsequently slightly adapted in WaterGAP 2.2. The reservoir storage S_r increases with inflow I from other storages or from upstream, and is reduced by the outflow Q. In case of irrigation reservoirs, the outflow is computed as a function of downstream water demand. Additionally, reservoir water balance storage is affected by precipitation P and potential evaporation E_w applying an albedo of 0.08. Finally, net abstractions NA_s are withdrawn (Eq. 1).

$$\frac{dS_r}{dt} = I - Q + P - E_w - NA_s \qquad (1)$$

Reservoir evapotranspiration is reduced with decreasing reservoir storage. If reservoir storage falls below 10% of its storage capacity, the release coefficient is set to 0.1, assuring water release for downstream ecosystem demands. The reservoir algorithm is also applied to natural lakes that are regulated by dams. In its current version, the algorithm does not include reservoir commissioning years, i.e. all reservoirs are assumed to have existed since 1901.

Groundwater storage. Groundwater storage S_g increases with groundwater recharge R_g and is decreased by base flow Q_g and net groundwater abstraction NA_g (Eq. 2).

$$\frac{dS_g}{dt} = R_g - Q_g - NA_g \qquad (2)$$

Groundwater recharge is calculated as a fraction of runoff from land, according to relief, soil texture, aquifer type and the existence of permafrost or glaciers. Additionally, it is assumed that in semiarid and arid areas, groundwater recharge from surface water bodies occurs (Döll et al. 2014b). Net groundwater abstraction NA_g is equal to groundwater withdrawals minus return flow from irrigation with both surface water and groundwater. Therefore, NA_g can also act as an inflow (e.g. as additional groundwater recharge due to irrigation with surface water).

[1] See CCI Sea Level Budget Closure Proposal, section “WP250 Land water contribution”.

Glacier storage. WaterGAP 2.2b does not compute glacier water storage variations. However, in a non-standard version of a former version of WaterGAP 2.2, daily output time series of the global glacier model HYOGA2 (glacier area, glacier mass, glacier runoff; Hirabayashi et al. 2013; Hirabayashi et al. 2010) were integrated to better simulate river discharge downstream of glaciers.

6.3. Product Specification

6.3.1. Product geophysical data content

The data products consist of global and gridded time series of TWS variations that depend on individual variations of canopy storage S_c, snow water storage S_{sn}, soil storage S_s, groundwater storage S_g and surface water bodies storages S_{swb} (Eq. 3).

$$\frac{dTWS}{dt} = \frac{S_c}{dt} + \frac{S_{sn}}{dt} + \frac{S_s}{dt} + \frac{S_g}{dt} + \frac{S_{swb}}{dt} \qquad (3)$$

6.3.2. Coverage and resolution in time and space

WaterGAP 2.2b calculates daily water flows and storages at a spatial resolution of 0.5°x0.5° (approximately 55 km by 55 km at the equator) for the whole land area of the globe except Antarctica. For version 0 data products, monthly and annual time series of globally averaged TWS, as well as 0.5°x0.5° gridded monthly time series of TWS were computed by the model for 1992-2014. Note that for the globally averaged time series, Greenland was excluded and an area-weighted average was used. Weighting areas are so-called "continental areas" that in case of coastal cells exclude the part of the 0.5°x0.5° grid cell that is ocean (see 6.3.4).

6.3.3. Product data format

The gridded time series of TWS are provided in a NetCDF format (compressed and uncompressed). Daily WFDEI (Watch Forcing Data based on ERA-Interim reanalysis) climate forcing was used as input data, as it gives the best fit to observed times series of monthly river discharge (Müller Schmied et al. 2014). The globally averaged time series of TWS are provided for three climate forcings (see 6.4.4), including the daily WFDEI climate forcing, in an Excel and text format.

6.3.4. Product grid and projection

The WATCH-CRU ocean-land mask, covering 67420 0.5°x0.5° grid cells, was used for the simulations.

6.3.5. Data files provided

Times series of global TWS are provided by the files

global_tws \ WaterGAP22b_*FORCING*_version0_*time*1992_2014.txt

with *FORCING*: CRU, CRUGPCC, WFDcbWFDEI
and time: month, year, year in month,

and

global_tws \ global_average_tws_without_greenland.xls.

Column 1: Time (Month-Year)
Columns 2-7: TWS as computed by the model with different forcings: WFDEI, CRU, CRUGPCC, given are monthly and yearly mean values
Columns 8-13: TWS as in Columns 2-7, but time series are normalized with respect to the time series mean values (TWS – time series mean)

Gridded data are available by **tws_WaterGAP22b_WFDEIhom_version0.nc/nc4**

Geophysical Variable	Name in product	Unit
total water storage forced by homogenized WFD WFDEI forcing	tws	mm

6.4. Uncertainty Assessment

6.4.1. Sources of error

The uncertainty in simulated TWS variations is due to the spatially distributed input data, in particular climate forcing and land cover, the model structure, the modeling approach (e.g. consideration or not of human water use) and the calibration approach (see 6.2.1), as well as the many parameters used in the model.

6.4.2. Methodology for uncertainty assessment

To assess the sensitivity of simulated global-scale freshwater flows[2] and TWS variations to the sources of error mentioned above, six model variants were designed (Müller Schmied et al. 2014). The standard version of WaterGAP 2.2 (STANDARD) was modified regarding only one aspect, including either alternative climate forcing (CLIMATE), alternative land cover input (LANDCOVER) or a simplified model structure (STRUCTURE). In addition, variant NoCal was

[2] River discharge Q, renewable water resources RWR and actual evapotranspiration AET.

an uncalibrated simulation with the standard version and variant NoUse was a simulation without consideration of the impact of human water use. Dominant uncertainties were determined by calculating differences between the values computed with a certain model variant and STANDARD. Furthermore, in Müller Schmied et al. (2016a), the uncertainty due to climate input data on global water balance components was assessed by forcing WaterGAP with five state-of-the-art climate forcings.

6.4.3. Results of uncertainty assessment

The global TWS trend (row 3 in Table 7) is most sensitive to STRUCTURE and NoUse, as these model variants do not reflect groundwater depletion. The basin-specific calibration to observed mean annual river discharge (NoCal) ranks third (Table 7). All WaterGAP simulations done within the project will be done with calibrated model versions. Concerning human water use, the related uncertainty will be determined by applying various plausible water use variants, with a focus on irrigation water use. As for uncertainty due to model structure, it may be assessed at a later stage of the project, once some model developments have been implemented. Furthermore, uncertainty due to climate forcing will be assessed by using an ensemble of climate datasets, as has been done by Müller Schmied et al. (2016a).

Precipitation uncertainty is one of the most important factors of climate forcing uncertainty. Table 8 shows that total precipitation variations are large among the different climate forcings used by Müller Schmied et al. (2016a). Nevertheless, the impact on global TWS variations (row 5) remains low as the latter represent only a very small percentage of total precipitation. Relative uncertainties for smaller spatial units are much higher than for global values.

Table 7: The three model variants with the largest differences to the STANDARD variant (dSTA) regarding global freshwater fluxes (Q and AET) and total water storage trends (dTWS/dt) (values in km³/yr) as well as median E_{NS}[3] for monthly time series of river discharge at the 1319 calibration basins. For details see Müller Schmied et al. (2014).

Variable	STANDARD	Rank 1	dSTA	Rank 2	dSTA	Rank 3	dSTA
Q	40 458	NoCal	6364	CLIMATE	1906	NoUse	758
AET	69 803	NoCal	−6459	STRUCTURE	414	LANDCOVER	209
$dTWS/dt$	−214	STRUCTURE	169	NoUse	140	NoCal	71
Median E_{NS}	0.54	NoCal	−0.66	STRUCTURE	−0.05	CLIMATE	−0.03

[3] Spatial distribution of Nash-Sutcliffe Efficiency.

Table 8: Global water balance components for land area (except Antarctica and Greenland) in % of precipitation (row 1 lists absolute precipitation values) for the five model variants and 1971-2000. Cells representing inland sinks were excluded but discharge into inland sinks was included. For details see Müller Schmied et al. (2016a).

No.	Component	GSWP3	PGFv2	WFD	WFDEI_hom	WFD_WFDEI
1	Precipitation P ($km^3 yr^{-1}$)	109 631	103 525	110 690	111 050	111 050
2	Actual evapotranspiration AET[a]	62.0	61.3	61.1	63.0	62.0
3	Discharge into oceans and inland sinks Q^b	37.1	37.8	38.1	36.2	37.2
4	Water consumption (actual) WCa	0.9	0.9	0.8	0.9	0.8
5	Change of total water storage dS / dt^c	−0.01	−0.03	−0.02	−0.02	−0.07

[a] AET does not include evapotranspiration caused by human water use, i.e. actual water consumption WCa. [b] Taking into account anthropogenic water use.
[c] Total water storage (TWS) of 31 December 2000 minus TWS of 31 December 1970, divided by the number of 30 years.

6.4.4. Uncertainty documentation in the data products

WaterGAP was forced by three state-of-the-art climate forcings; daily WFDEI dataset (Weedon et al. 2014, based on ERA-Interim reanalysis, with, among other corrections, precipitation bias-corrected using GPCC (until 2013) and CRU TS (for 2014) monthly precipitation sums, see details in http://www.eu-watch.org/gfx_content/documents/README-WFDEI%20(v2016).pdf), monthly CRU TS 3.23 (Harris et al. 2014) and monthly CRU TS3.23 with precipitation sums replaced by GPCC v7 (Schneider et al. 2015) until 2013. Figure 17 shows that absolute total water storages of WFDEI forcing are lower than those computed with CRU and CRUGPCC. This can be attributed on the one hand due to lower global averages of precipitation (WFDEI: 848 mm/yr, CRU: 868 mm/yr, CRUGPCC: 860 mm/yr) and on the other to a strongly different storage level of Lake Malawi (30 mm difference) due to local differences of climate forcing (net radiation). However, in relative terms or amplitudes, global mean TWS is not very dependent on climate forcing (Figure 18). At grid cell level, climate forcing tends to have a larger impact on water balance components (Müller Schmied et al. 2016a).

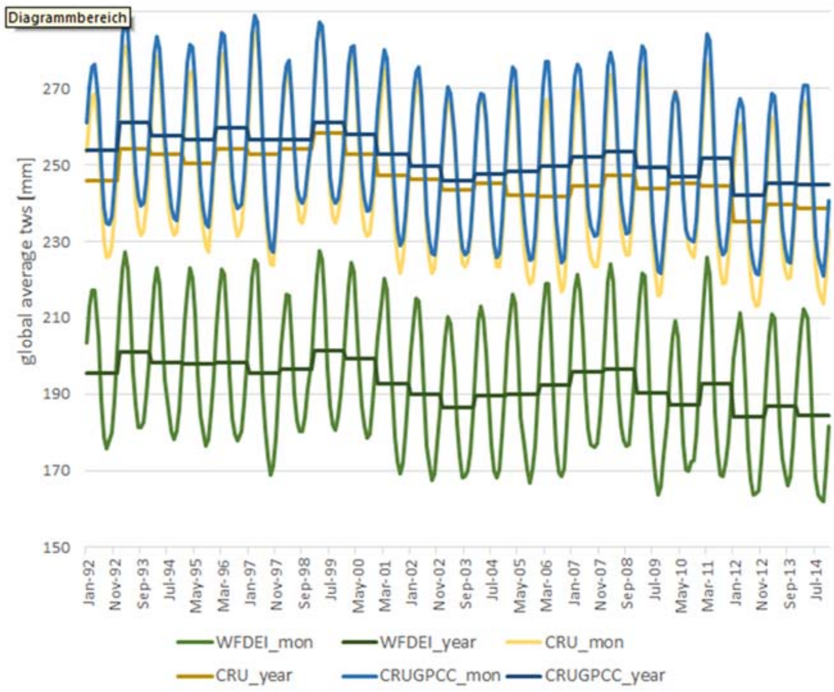

Figure 17: Global average for land area (except Antarctica and Greenland) in mm of monthly and annual total water storage variations for three climate datasets and 1992-2014.

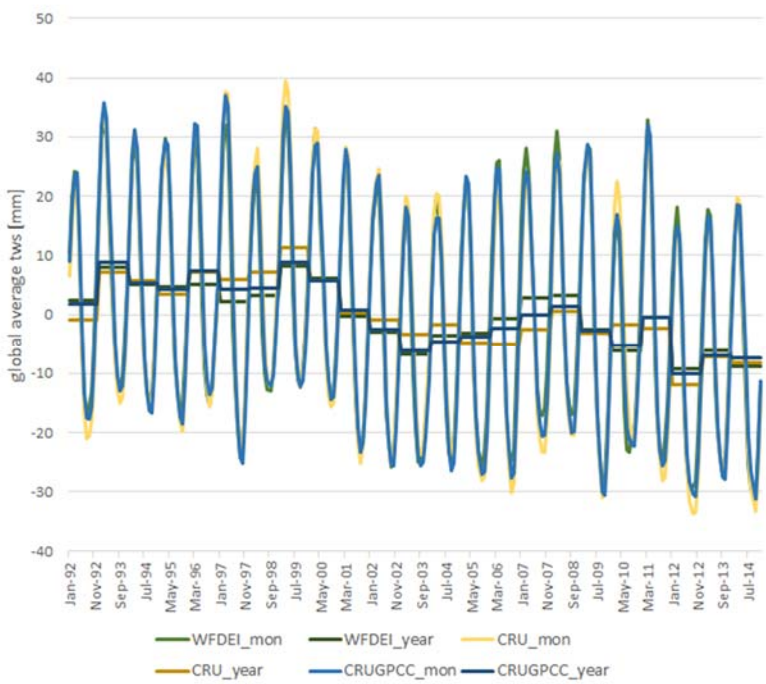

Figure 18: Global average for land area (except Antarctica and Greenland) in mm of monthly and annual total water storage variations for the three climate data sets and 1992-2014. Here, relative values were calculated by removing the mean value of each dataset.

6.5. References

Chao, B. F.; Wu, Y. H.; Li, Y. S. (2008): Impact of artificial reservoir water impoundment on global sea level. In *Science (New York, N.Y.)* 320 (5873), pp. 212–214. DOI: 10.1126/science.1154580.

Döll, P.; Fiedler, K.; Zhang, J. (2009): Global-scale analysis of river flow alterations due to water withdrawals and reservoirs. In *Hydrol. Earth Syst. Sci. Discuss.* 6 (4), pp. 4773–4812. DOI: 10.5194/hessd-6-4773-2009.

Döll, P.; Fritsche, Mathias; Eicker, Annette; Müller Schmied, Hannes (2014a): Seasonal Water Storage Variations as Impacted by Water Abstractions: Comparing the Output of a Global Hydrological Model with GRACE and GPS Observations. In *Surv Geophys* 35 (6), pp. 1311–1331. DOI: 10.1007/s10712-014-9282-2.

Döll, P.; Hoffmann-Dobrev, H.; Portmann, F. T.; Siebert, S.; Eicker, A.; Rodell, M. et al. (2012): Impact of water withdrawals from groundwater and surface water on continental water storage variations. In *Journal of Geodynamics* 59-60, pp. 143–156. DOI: 10.1016/j.jog.2011.05.001.

Döll, P.; Lehner, Bernhard (2002): Validation of a new global 30-min drainage direction map. In *Journal of Hydrology* 258 (1-4), pp. 214–231. DOI: 10.1016/S0022-1694(01)00565-0.

Döll, P.; Müller Schmied, Hannes; Schuh, Carina; Portmann, Felix T.; Eicker, Annette (2014b): Global-scale assessment of groundwater depletion and related groundwater abstractions: Combining hydrological modeling with information from well observations and GRACE satellites. In *Water Resour. Res.* 50 (7), pp. 5698–5720. DOI: 10.1002/2014WR015595.

Hanasaki, Naota; Kanae, Shinjiro; Oki, Taikan (2006): A reservoir operation scheme for global river routing models. In *Journal of Hydrology* 327 (1-2), pp. 22–41. DOI: 10.1016/j.jhydrol.2005.11.011.

Harris, I.; Jones, P.D; Osborn, T.J; Lister, D.H (2014): Updated high-resolution grids of monthly climatic observations - the CRU TS3.10 dataset. In *Int. J. Climatol.* 34 (3), pp. 623–642. DOI: 10.1002/joc.3711.

Hirabayashi, Yukiko; Döll, P.; Kanae, Shinjiro (2010): Global-scale modeling of glacier mass balances for water resources assessments. Glacier mass changes between 1948 and 2006. In *Journal of Hydrology* 390 (3-4), pp. 245–256. DOI: 10.1016/j.jhydrol.2010.07.001.

Hirabayashi, Yukiko; Zang, Yong; Watanabe, Satoshi; Koirala, Sujan; Kanae, Shinjiro (2013): Projection of glacier mass changes under a high-emission climate scenario using the global glacier model HYOGA2. In *Hydrological Research Letters* 7 (1), pp. 6–11. DOI: 10.3178/hrl.7.6.

Müller Schmied, H.; Eisner, S.; Franz, D.; Wattenbach, M.; Portmann, F. T.; Flörke, M.; Döll, P. (2014): Sensitivity of simulated global-scale freshwater fluxes and storages to input data, hydrological model structure, human water use and calibration. In *Hydrol. Earth Syst. Sci.* 18 (9), pp. 3511–3538. DOI: 10.5194/hess-18-3511-2014.

Müller Schmied, Hannes; Adam, Linda; Eisner, Stephanie; Fink, Gabriel; Flörke, Martina; Kim, Hyungjun et al. (2016a): Impact of climate forcing uncertainty and human water use on global and continental water balance components. In *Proc. IAHS* 374, pp. 53–62. DOI: 10.5194/piahs-374-53-2016.

Müller Schmied, Hannes; Müller, Richard; Sanchez-Lorenzo, Arturo; Ahrens, Bodo; Wild, Martin (2016b): Evaluation of Radiation Components in a Global Freshwater Model with Station-Based Observations. In *Water* 8 (10), p. 450. DOI: 10.3390/w8100450.

Schneider, Udo; Becker, Andreas; Finger, Peter; Meyer-Christoffer, Anja; Rudolf, Bruno; Ziese, Markus (2015): GPCC Full Data Reanalysis Version 7.0 at 0.5°: Monthly Land-Surface Precipitation from Rain-Gauges built on GTS-based and Historic Data. DOI: 10.5676/DWD_GPCC/FD_M_V7_050.

Wada, Yoshihide; van Beek, Ludovicus P. H.; Sperna Weiland, Frederiek C.; Chao, Benjamin F.; Wu, Yun-Hao; Bierkens, Marc F. P. (2012): Past and future contribution of global groundwater depletion to sea-level rise. In *Geophys. Res. Lett.* 39 (9), L09402. DOI: 10.1029/2012GL051230.

Weedon, Graham P.; Balsamo, Gianpaolo; Bellouin, Nicolas; Gomes, Sandra; Best, Martin J.; Viterbo, Pedro (2014): The WFDEI meteorological forcing data set. WATCH Forcing Data methodology applied to ERA-Interim reanalysis data. In *Water Resour. Res.* 50 (9), pp. 7505–7514. DOI: 10.1002/2014WR015638.

7. Arctic Sea Level Change

7.1. Data Access and Requirements

To describe the changes in the Arctic sea level as seen from satellite altimetry we use the sea level anomaly (SLA) given in the DTU Arctic altimetric sea level record. Version 3 of this record can be obtained from the public ftp-server: ftp://ftp.space.dtu.dk/pub/ARCTIC_SEALEVEL/V3/MONTHLY_GRIDDED/.

In addition data on both sea level change and steric sea level change are also obtained from the TOPAZ4 data assimilation system operated at NERSC. This system represents the Arctic Marine Forecasting Center of the Copernicus Marine Services (http://marine.copernicus.eu/). The system delivers routinely products and information used for analyses, forecast (up to 10 days) and reanalyses.

7.2. Algorithms

7.2.1. Review of scientific background

DTU Arctic Altimetric Sea Level Record: The SLAs are derived from satellite altimetry by measuring the distance between the satellite and the underlying surface using a radar altimeter. By measuring this distance and using the exact position of the satellite obtained through GPS, the height of the underlying surface referenced to the ellipsoid can be estimated. SLAs are referenced to the mean sea surface (MSS).

NERSC TOPAZ4: NERSC TOPAZ4 is a coupled ocean and sea ice data assimilation system for the North Atlantic and the Arctic Ocean that is based on the Hybrid Coordinate Ocean Model (HYCOM) and the Ensemble Kalman Filter data assimilation [Sakov et al. 2012]. HYCOM is using 28 hybrid z-isopycnal layers at a horizontal resolution varying from 16 km in North Atlantic to 12 km in the Arctic Ocean. The TOPAZ4 system is forced by the ECMWF ERA Interim reanalysis and assimilates most available measurements including along-track altimetry data, sea surface temperatures, sea ice concentrations and sea ice drift from satellites along with in-situ temperature and salinity profiles from Argo floats and research cruises. For validation results and more details see Sakov et al., [2012] and Xie et al., [2017].

7.3. Product Specification

7.3.1. Product geophysical data content

DTU Arctic Altimetric Sea Level Record: The data consists of SLAs from the DTU Arctic sea level record. The Arctic record comprise ERS-1, ERS-2, ENVISAT and CryoSat-2 altimetry data. The data were tailored, edited and processed according to Cheng and Andersen (2015), and are referenced to the DTU13 Mean Sea Surface (Andersen et al., 2015).

NERSC TOPAZ4: The TOPAZ4 products contain sea surface height (meters; relative to geoid), and steric height (meters).

7.3.2. Coverage and resolution in time and space

DTU Arctic Altimetric Sea Level Record: The Arctic SLAs are available in the region 66°N - 82°N from September 1992 to August 2014. The final data product is given as monthly gridded values. Figure 19 shows the percentage of available weekly observations compared to the entire DTU Arctic sea level dataset. The availability of data depends primarily on the presence of sea ice.

NERSC TOPAZ4: The TOPAZ4 covers the North Atlantic and entire Arctic Oceans bounded by 20 - 90°N and 180°W to 180°E with a spatial resolution of 0.125°. The temporal coverage is from 2003-2015 at a monthly resolution.

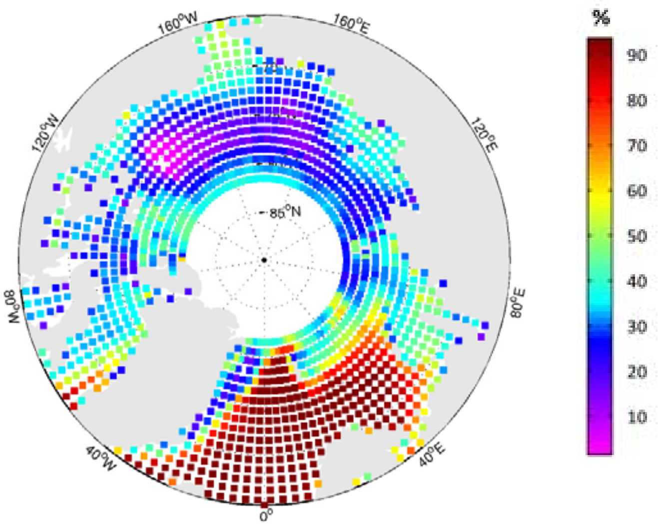

Figure 19: Percentage of weekly altimetric observations

7.3.3. Product data format

<u>*DTU Arctic Altimetric Sea Level Record:*</u> The monthly SLA data are given in ASCII format. Each file holds a series of monthly mean SLAs for which the year and month is specified in the filename, which has the form: "*Arc_SLA_YYYYMM.dat.gz*". The data files have five data columns holding

value1	latitude [°]	longitude [°]	*value4*	height [m]

For grid cells without data the SLA is set to 10000. Columns 1 and 4 contain values not used as data (*value1* and *value4* to be ignored).

<u>*NERSC TOPAZ4:*</u> The format of the TOPAZ4 fields is in NetCDF CF 1.0. Dimensions are 2881 in longitude and 561 in latitude and 156 in time, and variables are SSHTOP and STERICHT.

Files: (1) topazssh20032015.nc
(2) topazstht20032015.nc

Geophysical Variable	**Name in product**	**Unit**
Longitude	LONGITUDE	degrees_east
Latitude	LATITUDE	degrees_north
Time	TAX	months since 1901-01-15 00:00:00
(1) Sea Surface Height (2) Steric Sea Level	SSHTOP STERICHT	m m

7.3.4. Product grid and projection

<u>*DTU Arctic Altimetric Sea Level Record:*</u> The SLA data are given in a 0.5°x0.5° resolution.

<u>*NERSC TOPAZ4:*</u> The TOPAZ4 is provided on a regular 0.125°x0.125° latitude-longitude grid.

7.4. Uncertainty assessment

<u>*DTU Arctic Altimetric Sea Level Record:*</u> Estimation of the Arctic SLAs is challenged by the presence of sea ice and off-nadir reflections as well as uncertainties from data editing.

<u>*NERSC TOPAZ4:*</u> The sources of error come predominantly arise from deficiency in the TOPAZ4 model system and lack of in-situ data for assimilation.

7.5. References

Andersen O. B., Knudsen, P., Stenseng, L. (2015). The DTU13 MSS (Mean Sea Surface) and MDT (Mean Dynamic Topography) from 20 Years of Satellite Altimetry. *International Association of Geodesy Symposia*, Springer International Publishing Switzerland, DOI 10.1007/1345_2015_182.

Cheng Y., Andersen O. B., Knudsen P. (2015). An Improved 20- Year Arctic Ocean Altimetric Sea Level Data Record, *Marine Geodesy*, 38:2, 146-162, DOI: 10.1080/01490419.2014.954087.

Sakov, P., F. Counillon, L. Bertino, K. A. Lisæter, P. R. Oke, and A. Korablev (2012) TOPAZ4: an ocean-sea ice data assimilation system for the North Atlantic and Arctic. *Ocean Science*, 8:633-656, doi:10.5194/os-8-633-2012.

Xie, J., L. Bertino , F. Counillon, K. A. Lisæter, and P. Sakov (2017), Quality assessment of the TOPAZ4 reanalysis in the Arctic over the period 1991-2013, *Ocean Sci*., 13(1), pp. 123-144, doi:10.5194/os-2016-38, 2016 doi:10.5194/os-13-123-2017.

Attachments

ESA_SSL4SLBC_cci_D2.1.2

Steric Sea Level for Sea Level Budget Closure Product Description Document 1 (submitted to ESA 2017-05-25, revised 2017-09-27)